FINE-SCALE OBSERVATIONS OF SURFACE BOUNDARIES UTILIZING MOBILE MESONETS

by

ALBERT EDWARD PIETRYCHA, B.S.

A THESIS

IN

ATMOSPHERIC SCIENCE

Submitted to the Graduate Faculty
of Texas Tech University in
Partial Fulfillment of
the Requirements for
the Degree of

MASTER OF SCIENCE

Approved

ACKNOWLEDGEMENTS

I would like to acknowledge with gratitude my advisor and committee chairman, Dr. Arthur Doggett, and my committee members, Dr. Richard Peterson and Dr. Erik Rasmussen. A special *thank you* to Dr. Erik Rasmussen for his insight, guidance, and exceptional example, for providing me with a plethora of unique research opportunities, and for his unfailing support of the research effort documented herein. I am also grateful to Dr. Lance Bosart for his review and comments with Hurricane Floyd, and to Dr. Franks Marks and Mr. Michael Black, at HRD, for providing the dropsonde data. I would like to thank the Texas Tech Atmospheric Science students, as well as many other individuals for their assistance in this research. Without their contributions, a considerable portion of the data presented herein would not have been possible.

To Ms. Elke Ueblacker, I am indebted for untold hours of assistance and the patience with which she has endured aiding me in all my manuscript preparations.

Finally, heartfelt thanks to Walter, Marilyn, Glenn, and Heather Pilipski, for their support and love at a time in my life when I needed it the most. Without their nurture, I could not have come this far.

TABLE OF CONTENTS

ABSTRACT

Over the past decade, technological advances have permitted observations of the atmosphere in fresh and innovative ways. Observational platforms have been created and improved allowing atmospheric sampling, both remotely and via in situ data collection. Information gained from new platforms has aided the meteorological community to better understand an abundance of atmospheric thermodynamic, kinematic, and dynamic issues. Recently, a growing emphasis has been placed on investigation of the fine-scale structure of meteorological phenomena such as hurricanes, severe thunderstorms, drylines, and other boundaries. To provide the required resolution these investigations demand, a mobile observing platform, dubbed the mobile mesonet, was designed specifically for the sampling of small-scale features. The mobile platform was originally employed in the study of tornadoes and severe local storms. However, applications since have expanded to include a profusion of atmospheric surface features.

This thesis presents a case study, exceptional in that it incorporates mobile mesonet observations. Included are the investigations of a low-level baroclinic zone interaction with Hurricane Floyd in 1999. The presentation of data and analyses also serve to illustrate the unparalleled capabilities and versatility of the mobile mesonet in resolving surface features in scales heretofore indistinguishable in atmospheric research.

LIST OF FIGURES

CHAPTER I

INTRODUCTION

Observational meteorology is often faced with challenging questions regarding the most effective methods for sampling specific atmospheric features at varying scales. As our knowledge and understanding of the atmosphere increases, a disproportional number of fresh questions and hypotheses arise. In an attempt to address some of these challenges and to refute or verify hypothesis, new observational platforms are continually being designed and applied. In past studies, common observational platforms included portable and fixed soundings, measurements obtained by aircraft, portable and ground fixed radars, surface mesonet sites, standard surface airways observations, satellite imagery, and profiler data. Although these platforms have provided data sets that furthered the understanding of fine-scale features and structure, none have allowed the flexibility nor logistic availability required to readily sample scales less than observable with the older observational networks in both in time and space.

Recently, an emphasis has been placed on obtaining fine-scale observations of small-scale weather phenomena such as drylines, frontal boundaries, hurricane structure, and severe local storms. A new data collection platform was required to advance these goals and address the deficiencies of previous data collection attempts. One such mobile weather observing system, dubbed the mobile mesonet (MM) (Straka et al. 1996), was designed for accurate, high resolution, in situ meteorological observations. MMs have been employed in various field efforts, ranging from convective initiation studies to

deployment in hurricanes. The benefits derived from the MM have included the identification of spatial and temporal characteristics of surface features with horizontal scales on the order of tens of meters to ten kilometers. In this chapter, a brief background of the MM and accompanying analysis techniques are presented.

1.1 Mobile Mesonet Description

The MM design was developed out of a necessity to support the objectives of the Verification of the Origins of Rotation in Tornadoes Experiment (VORTEX; Rasmussen et al. 1994). As stated by Straka et al. (1996), the MMs were designed for use in making fine-scale meteorological observations of various phenomena associated with thunderstorms, surface boundaries (e.g., fronts, drylines), shear lines, and various small-scale weather phenomena. A MM consists of a suite of sensors fastened to an instrument rack and mast affixed atop the roof of a standard automobile, and a data collection, storage and display system (Fig. 1.1). The sensor suite records air pressure, temperature, relative humidity, and 3-meter wind speed and direction. A flux-gate compass is used to provide vehicle heading when the vehicle is stationary. A Global Positioning System (GPS) receiver is utilized providing the vehicle's position, universal time coordinates (UTC), and mean vector motion when moving. The output from the sensors is hard wired into a programmable data logger for collection and processing, and stored in a laptop computer for later analysis. Software on the laptop allows the data to be readily displayed. The laptop display offers MM operators immediate information, which is employed to guide continual positioning adjustments, thereby placing the vehicles most

advantageously for data collection. The reader is referred to Straka et al. (1996) for a complete detailed description and discussion of the MM system.

The MM data are rigorously quality controlled before any analysis is performed. Quality control procedures are implemented using a series of computer correction algorithms. For data comparison a time period is selected when multiple MMs traveled together in close proximity, <1km, and meteorological conditions are quiescent. Data are output such that any gross reporting errors existing in the MM data, whether systematic or periodic, can be compared and analyzed to detect the source of the error. Once the source of the error has been identified, the erroneous data are either corrected or discarded. If the data output lies within levels of instrumentation error, and is in close agreement after comparison with the other MMs, it is deemed acceptable for analysis.

The MM data can be analyzed, either on a surface map as the data were collected, or a time-to-space (TS) conversion calculation can be applied (e.g., Fujita 1955; Fujita and Brown 1958; Fujita and Byers 1977). The TS technique is based upon Taylor's hypothesis. Under the assumption that turbulence is frozen as it advects past a sensor, the advection vector can be used to translate measurements as a function of time and space (Taylor 1938). Utilizing a TS conversion, the 2-dimensional (space) horizontal structure of the surface feature (e.g., front, dryline, tornado) can be analyzed based on 1-dimensional (e.g., E-W highway) data. To determine the correct translation vector for the conversion, the following minimization problem was solved objectively using a series of computing scripts. Where the vehicles are in close proximity (within 100 m) in TS converted space, they should be sensing very similar winds and thermodynamic

conditions. If they are not, either unsteadiness or an erroneously chosen translation velocity is implied and the data are being incorrectly positioned in the conversion process. By viewing the data in brief time interval windows on the order of minutes, it is possible to improve confidence such that extreme unsteadiness is not perceived to be a problem. The reference frame motion that gives the minimum mean absolute error for observations that are collocated in the reference frame is sought. For Hurricane Floyd, the minimum error was in temperature.

The observable scales of the MM range from tens of meters to tens of kilometers and are dependent on sampling strategy. Operating in a storm or feature relative framework the MMs perform transects that will produce the most advantageous data collection for the features of interest. With supercell data collection, vehicles are separated several kilometers apart traveling at ~18 m s^{-1}. The study of fine-scale structure along surface boundaries requires that the MMs are spaced under a kilometer apart and travel at varying speeds between ~18 m s^{-1} and ~2.24 m s^{-1}. A field coordinator oversees the MM operations and provides meteorological guidance to each vehicle in order to facilitate proper data collection.

1.2 Present Study

This thesis presents a case study in which MMs were employed to sample surface features of Hurricane Floyd. Chapter II discusses data sources and methods. Chapter III, Hurricane Floyd, introduces observations of the coastal front interaction with the hurricane. Chapter IV presents data and results of mesoscale and fine-scale observations

of the coastal front and Hurricane Floyd. Chapter V summarizes the thesis with recommendations for future MM hurricane investigations.

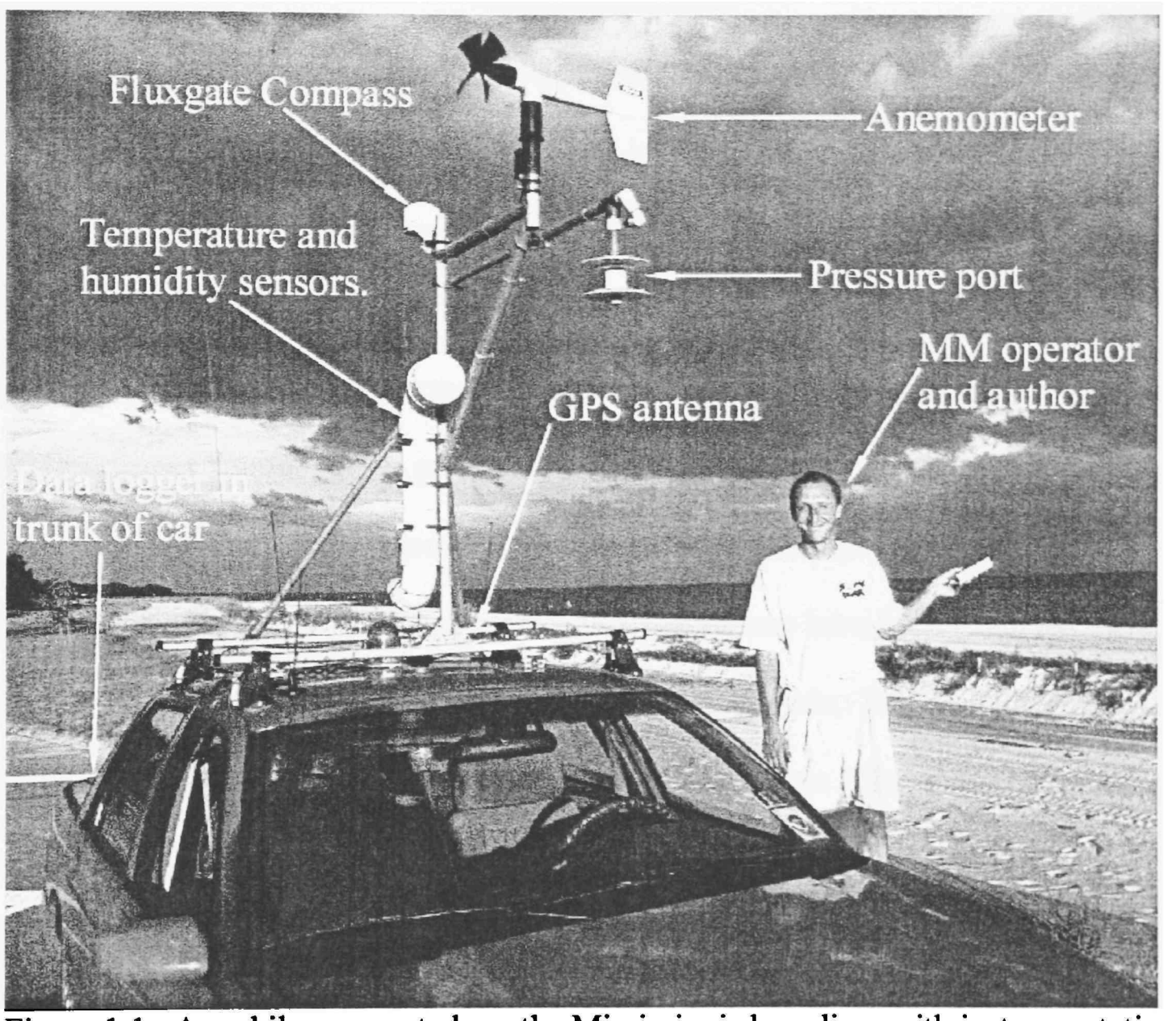

Figure 1.1. A mobile mesonet along the Mississippi shore line, with instrumentation labeled. The clouds in background are associated with the approach of Hurricane Georges, 26 September 1999.

CHAPTER II

DATA SOURCES AND METHODS

2.1 Surface Data

Surface data were obtained and analyzed for the period of 0900 UTC 15 September through 1200 UTC 16 September, inclusive (hereafter all times UTC). Hourly surface and moored buoy data were provided by the State University of New York at Albany (SUNYA). Data from all reporting stations were employed in subjective surface analysis. Stations generating erroneous data were omitted from analysis. To maintain time continuity for the figures provided herein, Automated Surface Observing System (ASOS) specials and Automated Weather Observing System (AWOS) observations generated during the minutes between hourly observations have been excluded. The observations, however, were included in the original analysis. The Franklin (FKN) and Suffolk (SFQ) AWOS were utilized for times series analysis. The AWOS observations were generated every 20 minutes with few data gaps for the time period analyzed. Neither station reported temperature in tenths Celsius. Hourly surface data were analyzed subjectively for temperature, dewpoint, sea level pressure, and wind fields. Coastal-Marine Automated Network (C-MAN) and ship data obtained by National Data Buoy Center, including buoy observations, were incorporated into the hourly plots to improve the spatial resolution over the ocean. MM data were overlaid in the surface plots to improve spatial resolution and analysis. Total deformation was computed using the

Rapid Update Cycle (RUC II) at the 1000 mb height. The intervals presented are times of model initialization.

2.2. Upper Air Analysis

Rawinsonde data evaluated within this analysis were obtained from SUNYA and the National Oceanic Atmospheric Administration Forecast Systems Laboratory (NOAA/FSL). Sounding data were used to create constant height and cross-sectional plots. These plots were then subjectively analyzed for synoptic and mesoscale features. Morehead City, NC (MHX), Greensboro, NC (GSO), and Roanoke, VA (RNK) (Fig. 2.1) soundings, launched at 0000 and 0600 on 16 September, were selected for frontal analysis. These sites were downstream of the hurricane and closest to landfall location. The lack of a complete 0000 GSO flight prevented analysis above 571 mb. MHX's 0600 sounding contained only mandatory levels through 400 mb. The 0000 MHX sounding was used to cross check the continuity of a 0600 MHX stability analysis, as discussed later. GPS dropsonde data obtained by the NOAA/AOML Hurricane Research Division (HRD) were also incorporated into this study. The final observations recorded before ocean splashdowns were utilized in the surface maps. Wind measurements from sondes 10, 11, 17, 18, and 29, as denoted in the HRD data set, were either missing or suspect and thus omitted from the surface overlays. In calculating the distance from a dropsonde to the eye, the center fixes for Floyd reported from the NOAA P3 and U.S. Air Force aircraft were utilized.

2.3 Radar Analysis

WSR-88D level II data (Crum et al. 1993) from MHX, Wilmington, NC (LTX), and Charleston, SC (CLX) were obtained from the National Climatic Data Center (NCDC). Data were processed on the WSR-88D Algorithm Testing and Display System (WATADS) version 10.1, developed by NSSL. The WSR-88D products selected for this study were velocity azimuth display wind profile (VAD), reflectivity, and velocity measurements. LTX was selected for analysis, as the radar was located closest to the area of landfall and level II data were available for the majority of the event, 1329 15 September to 1039 16 September, inclusive. Unfortunately, level II data from CLX and MHX were either not available or sporadic. To generate the VAD imagery a radius of 15 km was selected. At a radius of 30 km, the normal WSR-88D operational default, much of the data was missing as the hurricane approached the radar. The missing data were attributed to the inability of the interpretive algorithm to accurately differentiate the strong azimuthal shear associated with the hurricane's wind field (Smith 2000, personal communication). By selecting a 15 km radius, the algorithm was used to calculate wind profiles. Wind speeds and directions were compared to the limited available 30-km data with no gross errors detected. Most relevant to this study is the spatial rainfall distribution (as opposed to absolute rainfall amounts) illustrated by radar-derived storm total precipitation amounts.

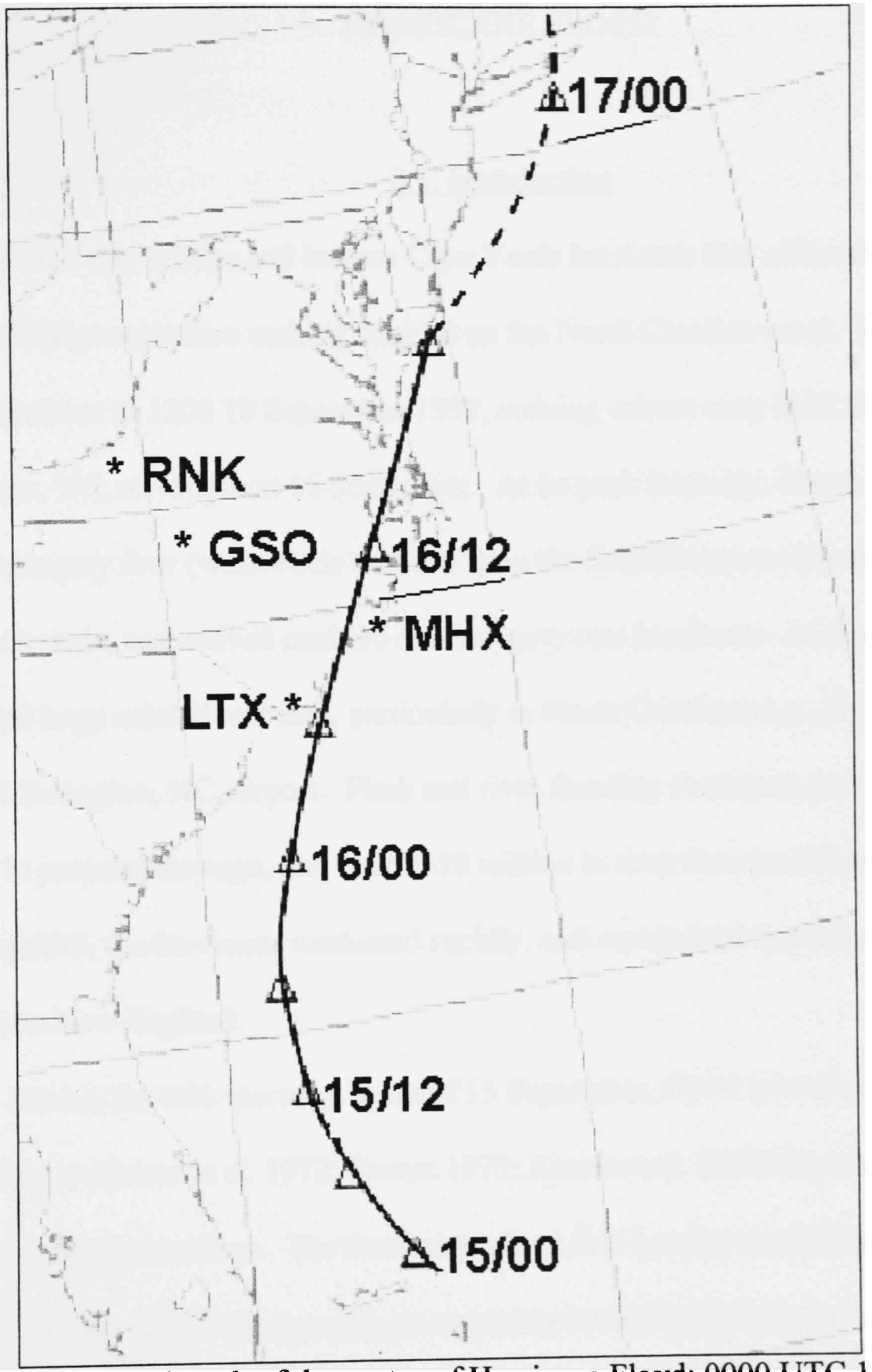

Figure 2.1. Partial track of the center of Hurricane Floyd; 0000 UTC 15 September-0000 UTC 17 September 1999. Day/time (UTC). Solid, and dashed lines denote hurricane and tropical storm stages of Floyd. Locations of key places mentioned in the text.

CHAPTER III

HURRICANE FLOYD

3.1 Introduction

Floyd was a large and intense Cape Verde hurricane that affected the central and northern Bahamas before making landfall on the North Carolina coast. Floyd attained hurricane force at 1200 10 September 1999, arriving ashore over Bald Head Island at Cape Fear, NC, at ~0630 on 16 September. At its peak intensity, Floyd reached the top end of category four (with winds >69 m s^{-1}) on the Saffir/Simpson (Simpson 1974) hurricane scale, and arrived onshore as a category two hurricane. At that time, Floyd produced large rainfall amounts, particularly in North Carolina; e.g., 48.4 cm of rain fell at the Wilmington, NC, airport. Flash and river flooding contributed to 40 fatalities, $1 billion in property damage, and over $150 million in crop damage (*Storm Data* 1999). After landfall, the hurricane weakened rapidly, and accelerated northward along the East Coast into New England.

During the mid-morning hours of 15 September, 12-15 hours before landfall, a coastal front (Bosart et al. 1972; Bosart 1975; Keeter et al. 1995; Garner 1999) developed over the eastern Carolinas. The thermal gradient first became established off the coast of South Carolina, with frontogenesis commencing immediately inland over the North Carolina coastline. The coastal front would propagate up the East Coast ahead of Floyd and into New England on 16 September (Bosart 2000, personal communication). Thermal and moisture gradients along the boundary intensified immediately downstream

(north) of the approaching hurricane. At the time of landfall the coastal front existed near the center of the hurricane. Concurrent with coastal front formation, Weather Surveillance Radar-1988 Doppler (WSR-88D) (Crum and Alberty 1993) reflectivity imagery over eastern North Carolina displayed the development of a persistent precipitation band in association with the front.

Previous observational (Bosart et al. 1972; Bosart 1975; Marks and Austin 1979; Keshishian and Bosart 1987) and numerical model (Ballentine 1980; Roebber et al. 1994) studies have documented that the heaviest rainfall amounts that occur in the vicinity of coastal fronts tend to occur along and just west of the boundary. Enhanced precipitation was attributed to a thermally direct circulation and associated convergence along the boundaries. Bosart and Dean (1991) demonstrated that the interaction between Tropical Storm Agnes, once a Gulf of Mexico hurricane, and a mesoscale thermal boundary east of the Appalachian Mountains was paramount in the production of excessive rainfall. Similar to the previously mentioned coastal front studies, the heaviest rains associated with Agnes occurred along and just west of the boundary. Recent investigations of rainfall rates (Bosart and Atallah 2000; Kong 2000) associated with Hurricane Floyd over the central Atlantic states and coastal sections of southern New England indicate that maximum precipitation amounts occurred just inland of the coastal baroclinic zone. Present analysis of Floyd's precipitation distribution in southeast North Carolina is in agreement with these studies. The greatest rainfall amounts were recorded along and to the west (cold) side of the coastal front boundary.

The National Severe Storms Laboratory (NSSL) and Texas Tech University participated in an experiment conducted during Hurricane Floyd. The project's primary objective addressed the issue of baroclinicity within the eyewall. The investigation was designed to document surface thermodynamics and kinematics embedded within the eyewall and eye. Objectives were achieved, in part, through the use of three data Mobile Mesonet (MM) systems. Incorporation of the MM observations with surface, rawinsonde, and in situ dropsonde data, indicated the boundary began interacting with the hurricane while the hurricane was offshore. This interaction produced a strong baroclinic structure within the west side of the hurricane that developed prior to through shortly after landfall and was associated with a precipitation maximum in North Carolina.

Prior to and during landfall, the MMs performed transects through the north and west portions of the eyewall and eye. Five hours before landfall, the MMs sampled the coastal front near North Myrtle Beach, SC (Fig. 3.1). Spanning the boundary, MM observations documented a temperature differential of 2.1°C over 5 km and a mixing ratio differential of 2.1 g kg^{-1} over 5 km. In situ MM and dropsonde (Fig. 3.1) samples resulted in sufficient data clarity to resolve the coastal front within the western eyewall immediately prior to landfall. A baroclinic zone was detected, extending across the western eyewall and into the eye. The MM data revealed a thermal gradient of 0.5°C km^{-1} over 5 km with a mixing ratio differential of 3.0 g kg^{-1} over the same distance. Concurrently, WSR-88D data displayed a rapid decline in the reflectivity distribution on the south and east side of the eyewall, and a transition toward weak radar echoes filling the eye. The combined data suggest that the hurricane began laterally entraining cooler

continental air while still offshore. Approximately 2.5 hrs after landfall, the center of Floyd became separated and secluded (Shapiro and Keyser 1990) from the maritime tropical air, its locus residing within a strong baroclinic zone.

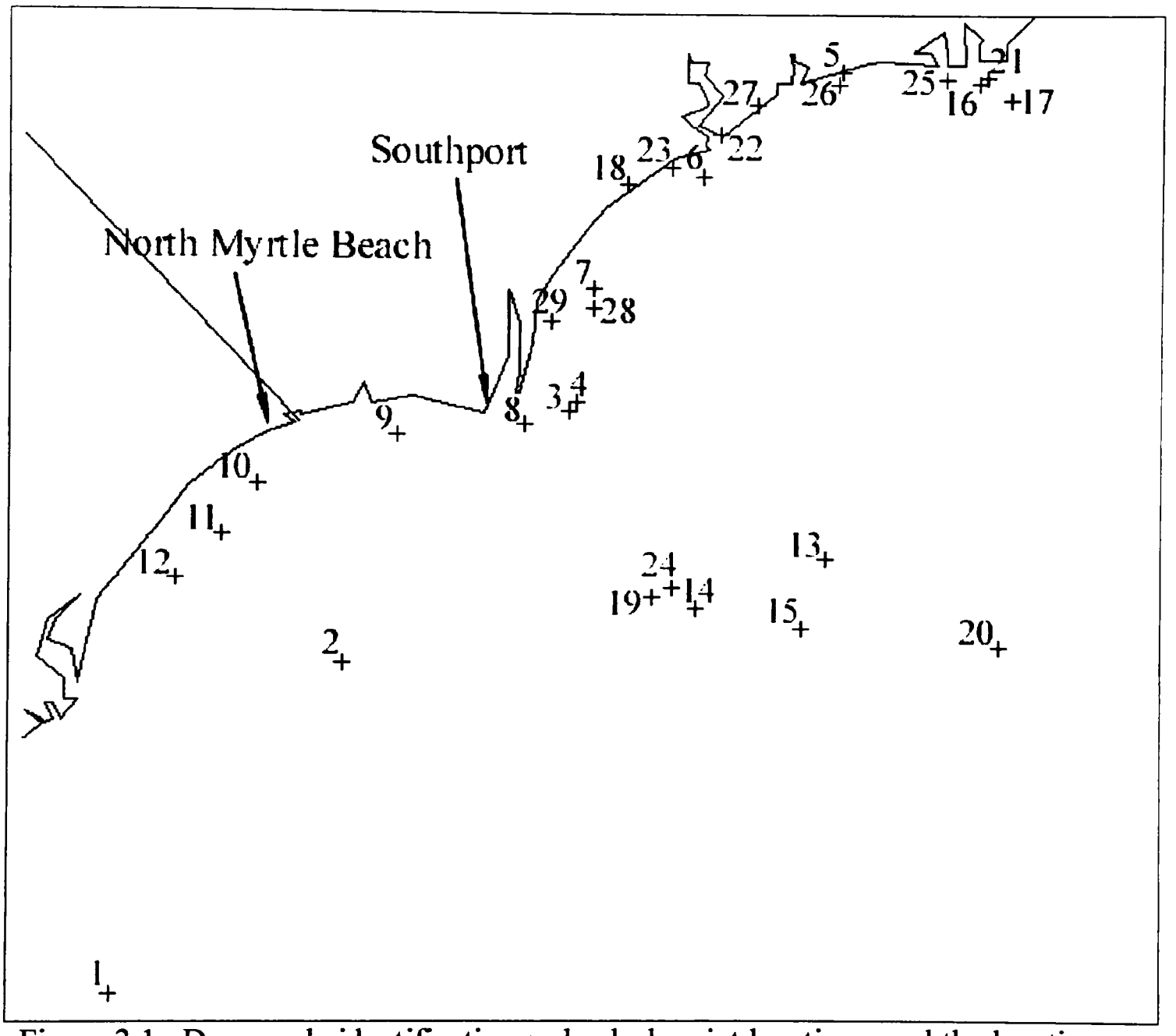

Figure 3.1. Dropsonde identification and splash point locations, and the locations of towns where mobile mesonet transects occurred.

CHAPTER IV

DATA AND RESULTS

4.1 Surface

Early on the morning of 15 September, an area with a diffuse low-level land-sea temperature gradient extended across the southern tidewater region of North Carolina. Hurricane Floyd was centered over the Atlantic ~500 km south of Cape Fear. As depicted in Figures 4.1-4.3, a north-south oriented coastal front developed by early afternoon and strengthened during the period prior to hurricane landfall. An inverted trough of low pressure advanced and persisted along the coastal front throughout the event.

Over the Atlantic, a warm moist airmass resided downstream of the hurricane, while relatively colder and drier air existed over the Eastern Seaboard and Appalachian Mountains, beginning in New England and extending southward in a narrow tongue to Jacksonville, FL. Cold air had dammed along the east-facing slopes of the Appalachian Mountains, a pre-existing condition favorable for the onset of coastal frontogenesis in New England (Bosart et al. 1972; Bosart 1975), as well as coastal fronts originating over the Carolinas and Virginia (Keeter et al. 1995).

These studies emphasized the importance of an anticyclone positioned north or northeast of the geographical location of interest. Cold air flowing around the anticyclone encounters the obstacle and accumulates along the slopes of the mountains. Keeter et al. (1995) state, "As the cold air builds up against the mountains, it is forced to

move southward, east of the barrier, as a 'wedge' of high pressure" (44). On the morning of 15 September, a 1027 mb anticyclone was centered offshore, southeast of Newfoundland, Canada (Fig. 4.4). The anticyclone may have contributed to the placement of a cooler and relatively drier airmass along the eastern slopes of the Appalachians, in contrast with the tropical airmass offshore of the Carolinas.

Additional cold air damming processes, as studied by Bosart and Dean (1991) during the landfall of Tropical Storm Agnes, played a more significant role in advecting the colder air southward, into the region near the Carolinas coastline. The surface cyclonic circulation associated with Agnes, combined with lower pressure along the coast, resulted in northerly surface winds. In such scenarios, cooler air is subsequently forced south on ageostrophic flow east of the Appalachian Mountains. Bosart and Dean compared this process to the regional cold-air damming scenario produced by the motion of a northern anticyclone as demonstrated by Forbes et al. (1987) and Bell and Bosart (1988). A temperature gradient of about 3°C 100 km^{-1} developed between this cool air and the tropical air immediately north of Agnes, which was advected westward (onshore) by the tropical storm.

Conditions akin to those of Agnes were present prior to the landfall of Hurricane Floyd. During the daylight and evening hours of 15 September, surface observations along the eastern slopes of the North Carolina Appalachians indicated temperatures 5-7°C cooler than the maritime air east of the front. The modest pressure differential of ~3 mb 100 km^{-1} east of the mountainous terrain in Carolina and Virginia was maintained by a strengthening 1023 mb anticyclone centered over the upper Midwest (Fig. 4.4).

Warm moist oceanic air, downstream of the hurricane, was advected westward on geostrophic winds toward the colder air. Meanwhile, the cold air was advected southward on ageostrophic flow. Surface pressure falls associated with this event were greatest along the coastline of the Carolinas due to the advancing storm, and within the trough of low pressure along the frontal zone (Figs. 4.1-4.3).

As Hurricane Floyd approached shore, the pressure gradient over the coastal plain intensified, accelerating the surface flow over the eastern Carolinas. The baroclinic zone associated with the temperature gradient strengthened, owing to increasing horizontal deformation (Figs. 4.5-4.8) and confluence (Bluestein 1993), but remained nearly stationary throughout the day. Frontogenesis continued further north, immediately inland from the shoreline and downstream of the advancing hurricane. By 0000 16 September, a coastal front oriented north-south was well established (Fig. 4.2), spanning the area east of Charleston, SC, to east of Virginia Beach, VA.

At 0124 on 16 September, three MMs intercepted the coastal front near the town of North Myrtle Beach, SC (Fig. 4.9), 5.5 hrs before the northern edge of the eye made landfall, and commenced sample collection. The MMs operated normal to the boundary for 25 min, on approximately the same latitude, and performed transects separated by 120 sec. Vehicle speeds were maintained at ~56 km h^{-1} during transects. This speed was selected to resolve horizontal thermal and kinematic gradients, and small-scale features embedded across the front. A 6-sec sampling rate while traveling at 56 km h^{-1} yields a spatial sampling interval of 93.6m. The front was observed to be moving west at 10 km h^{-1}. MM transects did not fully penetrate across the boundary as flooded roadways and

debris inhibited safe operations. Upon driving east after the transects, however, the eastern (warm) edge of the front was found to be ~4 km east of where the transects were conducted; air temperature east of the front maintained a nearly constant temperature ±0.5°C.

Analysis of the MM data revealed pronounced temperature (T), dewpoint (T_d), theta-e (θ_e), theta-v (θ_v), and mixing ratio (q) differentials across the front. Spanning a distance of ~5 km these were 2.1°C, 1.5°C, 9K, 1.7K, and 2.1 g kg^{-1}, respectively. The thermal gradient was relatively weak when compared with other coastal front studies documenting thermal contrasts of 10°C across 5-10 km (Bosart et al. 1972). The weaker thermal gradient could be a function of insufficient data: the use of only three MMs in this experiment limited sampling efforts across the full extent of the front. Three-meter winds measured by the MMs veered across the boundary from ~030° to ~360° with velocity nearly constant at 10 kt.

Keshishian and Bosart (1987) documented that ageostrophic flow over land and ahead of a cyclone enhances coastal convergence between cold continental air to the east of the Appalachian Mountains and the warm, moist air over the Atlantic Ocean. Using MM data collected near North Myrtle Beach and the centered differencing scheme, horizontal convergence values ($\partial u/\partial x + \partial v/\partial y$) at 0145 across the boundary were calculated at approximately -5.0×10^{-4} s^{-1}.

As Floyd approached the shore, surface winds intensified. The thermal gradient strengthened, owing to increasing confluence and horizontal total deformation along the boundary (Fig. 4.5-4.8). The secondary circulation associated with the front provided

additional lift along the boundary, thereby aiding in the development of sustained precipitation along the front. This process resulted in concentrated rainfall along and behind the boundary.

In addition to the MM data, observations from two AWOS sites were employed from locations in southeast Virginia, FKN and SFQ. These sites were spaced ~27 km apart and straddled the front. The data indicate a consistent thermal differential across the boundary. At both 0800 and 0900, the stations recorded the following T, T_d, and q difference across the front: 5°C, 6°C, and q 5.7 g kg^{-1}, respectively, with 80° backing of winds (Fig. 4.10).

Prior to landfall, the MMs moved to intercept the northern and western eyewall at Southport, NC. The MMs performed continuous transects at various vehicle speeds, traversing the area from the shoreline to ~20 km inland. The observed thermodynamic fields ahead of the approaching eyewall remained nearly homogeneous. Immediately before the western portion of the eyewall advanced over the tip of Cape Fear, the MMs were redeployed around the western eyewall. One MM remained stationary in the eye for a 55-min period, while the remaining MMs relocated to points inland. The maximum spatial separation between the MM within the eye and the MMs positioned farthest northwest was ~16 km (Figs. 4.11 and 4.12). The distances separating the vehicles allowed for limited storm-scale sampling of surface thermodynamic and kinematic changes within the eyewall. The front was observed, in conventional surface observations, to move rapidly eastward toward the shoreline as the eye approached Bald Head Island at Cape Fear. As the eye of the hurricane moved north-northeast along the

coastline, MM data clearly indicate an intrusion of colder and drier air into the eye of Floyd. At the time of landfall, 0630, the baroclinic zone sampled by the MMs was stronger than 5 hr previous near South Myrtle Beach. The horizontal gradients T, T_d, θ_e, θ_v, and q across ~5 km measured 2.4°C, 2.6°C, 12K, 2K, and 3.0 g kg^{-1}, respectively. The large baroclinic zone appears to have been a result of strong deformation. Additionally, convergence calculated from MM data was on an order of magnitude greater than that found 5.5 hr earlier along the front.

The evolution of the hurricane's surface environment is depicted in Figures 4.13-4.15. Based on the 0600 data (Fig. 4.13), the well-defined front surged eastward and entered the inner eyewall along the northwestern to southwestern quadrants of the system. By 0700 (Fig. 4.14), a distinct demarcation between the two airmasses north of the core existed. A seclusion of the hurricane system was imminent. Modified by sea-surface flux, the colder continental airmass traveled around the hurricane center and was advected well into the northeast quadrant. A narrow tongue of high θ_e (≥350 K) remained north of the eye; the remnant was subsequently advected southward.

Shapiro and Keyser (1990) produced a conceptual model describing four phases in frontal structure during the life cycle of extratropical cyclones. The model's fourth phase included the warm-core seclusion within the post-frontal polar air stream; cold air surges around the cyclone center, secluding a warm inner core. Numerous observational and numerical studies have documented extratropical seclusions (e.g., Donall et al. 1991; Neiman et al. 1991; Shapiro et al. 1991; Neiman and Shapiro 1993; Neiman et al. 1993). Based on the 0900 data, events akin to those presented by the above authors occurred as

Hurricane Floyd encountered the coast. The surface center of Floyd was severed from the tropical air and became immersed in the large baroclinic zone (Fig. 4.15). The hurricane's center became secluded, leaving a warm inner core.

North of Floyd's center, regional surface observations indicated the baroclinic zone along the coastal front contracted substantially (Fig. 4.15). Within the northwest, west and southwest quadrants of the hurricane and front, warming had occurred with a weakening of the thermal gradient and a westward retreat of the cold air. The cause of the warming is unknown, though one plausible explanation is mechanical mixing: the cold airmass was shallow (see next section) and overlain by warmer air, which may have mixed downward.

4.2 Upper Air

GSO and MHX released 0600 soundings on the night of 16 September (Fig. 4.16). The GSO sounding, launched deep inside the cold air west of the frontal boundary, indicated cold air with a depth of 1050 m, capped by a stable frontal inversion. A layer of dry air resided above the frontal inversion, between 850-700 mb. Based on satellite data (not shown), this layer was part of a narrow channel of dry air that was wrapped into and around the system from the southwest. A tropical airmass with a nearly moist adiabatic lapse rate was in place above the dry layer.

The GSO sounding contained no convective available potential energy (CAPE). East of the front and downstream of Floyd, the MHX sounding displayed a profile representative of a moist tropical airmass. The CAPE contained in the sounding was a

low ~210 J kg^{-1}. The thermal profile exhibited characteristics of convectively unstable thermal stratification ($\partial\theta_e/\partial Z < 0$) from 920 to 700 mb (Fig. 4.17). Comparison of the 0000 and the 0600 θ_e profiles indicates the instability in the thermal layer was likely greater at 0600 than was indicated due to the limited resolution (only mandatory levels) in the 0600 sounding.

Subjective cross-sectional analysis of potential temperature (Fig. 4.18) between RNK and MHX revealed cold air existed westward from the coastal front to the mountains of North Carolina and Virginia. Warm air advection (Fig. 4.16) and strong isentropic lift developed during the afternoon of 15 September over North Carolina, downstream of the hurricane, in the deep layer flow normal to the boundary (Fig. 4.19) and persisted as the storm moved onshore. Low- and mid-level tropospheric mesoscale slab ascent (Bryan and Fritsch 2000) over the front, of the moist convectively unstable layer was induced by the deep-layer flow, and contributed to heavy rainfall amounts immediately west of the front.

The NOAA P3 aircraft released 29 dropsondes between of the hours of 0441-0923 on 16 September. The respective sonde's nearest splash point observations are overlaid on Figures 4.13-4.15. The dropsonde data and subjective cross-sectional analysis of potential temperature (Fig. 4.20) revealed that the surface baroclinic structure in the western portion of Floyd was approaching the eyewall prior to landfall. The sixth, ninth and twelfth soundings were deployed in the northeast, northwest and west-southwest quadrants of the hurricane, respectively, at 0539, 0606, and 0614 (Fig. 4.13).

Dropsonde 6 (Fig. 4.21) was released 100 km northeast of the eye, ~70 km east of the coastal front. The data show a thermal profile containing an ~60 mb deep moist, absolutely unstable layer (MAUL) (Bryan and Fritsch 2000) from 940-880 mb. These thermal characteristics were similar to those measured by other dropsondes released near the same time in the east and northeast quadrant of the hurricane. Additionally, the thermodynamic profile was comparable to the 0600 MHX rawinsonde.

Dropsonde 12 (Fig. 4.21) indicated an ~1 km depth of cold air from the surface to 850 mb, accompanied by a pronounced frontal inversion. The airmass in this layer contained lower relative humidity than that observed with sonde 6. The vertical thermal profile was very similar to the 0600 GSO rawinsonde. Soundings 10 and 11 (not shown), flown immediately northeast of 12 in the western quadrant of the hurricane, contained similar thermodynamic profiles. All three dropsondes sampled the cold air and frontal inversion. Dropsonde 12 represents the westernmost sample, at a distance of ~84 km from the eye, and indicated the deepest cold air.

Dropsonde 9 (Fig. 4.22), released 29 km northwest of the eye, appeared to have fallen immediately on the cold side of the frontal boundary. A shallow frontal inversion was apparent in the lowest 60 m above the sonde's splash point. Based on the available data, the existence of the inversion is attributed to entrainment into the hurricane of the cold air that previously was present west of the coastal front. Though the sonde's cooler temperature readings were measured directly above the sea surface and might be construed as a reflection of seawater temperature, water temperatures ran 2-2.3°C warmer than the sonde's last reported temperature. Further, the environment was nearly

saturated, thus sharply limiting the amount of evaporative cooling caused by ocean spray. Dropsonde 8 (not shown), released 21 km north of the eye, 34 km east, and 14 min before sonde 9, contained no indication of cold air or an inversion. Additional evidence placing the sonde immediately west of the boundary was LTX radar data. By overlaying the sonde's splash point on the radar imagery, it became apparent that the sonde descended through the eastern edge of the frontal precipitation band.

During the period of 0638 to 0722, dropsondes 13 through 18 were sequentially released in the southeast and northeast quadrants. During that time, the data suggest that the coastal front had wrapped around the center of Floyd and into the northeast quadrant of the system (Fig. 4.14). Soundings 13 through 15 (Figs. 4.22 and 4.23) released in the southeast quadrant of the hurricane revealed that colder and drier air had traveled through that sector of the hurricane. Sounding 13, the easternmost sample, appeared closest to the eastward extent of the front; the sounding displayed the shallowest layer of cold air (~600 m deep). The depth of the cold air in sondes 14 and 15 was consistent with the sounding data in the west quadrant of the system.

From 0837 to 0923, sondes 24 through 29 (not shown) were released in the southwest, south, and northeast quadrants of the hurricane. Dropsonde thermodynamic profiles were similar to those flown earlier in the cold air west of the front. Dropsonde data, in conjunction with surface data (Fig. 4.15), indicated that within the lowest one kilometer, the center of Floyd had become secluded.

The dropsonde data incorporated with GSO, and MHX sounding data, resolved the boundary interactions incurred by Floyd with the coastal front before making landfall.

The data confirm the entrainment of relatively cold dry continental air into the northwest through southeast quadrants of the storm circulation prior to 0630 as seen in the surface analysis. By 0700, cold air had been wrapped northeast of the eye, drawing with it a narrow tongue of warm maritime tropical air from the north and directly toward the eye shortly after landfall. By 0900 the center of Floyd was secluded and resided within a large baroclinic zone.

4.3 Radar

During the morning and early afternoon of 15 September, the WSR-88D mosaic reflectivity indicated that the precipitation shield around Floyd was symmetrical and contained embedded 50-55 dBZ echoes north and east of a well-defined smooth eyewall. A broad area of nearly continuous 20-45 dBZ echoes extended from eastern South Carolina to eastern Virginia. Concurrent with the development of the coastal front, a band oriented north-south of enhanced 35-45 dBZ convective echoes developed along and immediately west of the coastal front. The frontal precipitation band was observed on the LTX radar, extending from ~76 km southeast of Charleston, SC, over the Atlantic, and into central North Carolina (Fig.4.24). The feature remained nearly stationary over North Carolina until immediately prior to hurricane landfall.

The spiral precipitation bands associated with Floyd maintained their spatial continuity east of the front. As the spiral bands rotated westward toward the coastal front, their discrete horizontal reflectivity structure was lost and became absorbed by the more uniform frontal precipitation band. Stronger convective cells (50-55 dBZ)

embedded within the spiral bands were observed to decrease in intensity and lose their reflectivity structure as the spiral bands crossed the boundary. This observation was intriguing and raised the question of what may have caused decrease in cell intensity prior to absorption by the front precipitation band.

As was shown in Figure 4.21, dropsonde 6, released in the northeast quadrant of the hurricane, resolved a ~60 mb MAUL. In a study of MAULs within mesoscale convective systems, Bryan and Fritsch (2000) produced a conceptual model demonstrating the occurrence of MAULs in regions of mesoscale slab ascent. Mesoscale slab ascent occurs in regions of strong vertical motion generated by mechanisms other than buoyancy driven acceleration. MAULs represent saturated layers within a slab; when these layers are lifted, the atmosphere is warmed due to latent heat release. Earlier studies, though not explicitly stated, have documented mesoscale slab ascent in association with squall lines (Roux 1988), mesoscale convective complexes (Smull and Augustine 1993; Trier and Parsons 1993), and warm fronts (Shapiro et al. 1991). Smull and Augustine (1993) demonstrated that inflow air glides above frontal surfaces in forced ascent. Trier and Parsons (1993) produced evidence of enhanced mesoscale ascent in association with a strong low-level jet; a layer of warm moist low-level air was lifted over a frontal surface by the low-level jet oriented normal to the frontal boundary (see also Fig. 22 Trier and Parsons 1993). Dynamically driven events tend to produce solid regions of radar echoes, as opposed to "cellular convection" (discrete echoes) (Bryan and Fritsch 2000).

Radar echoes intensities of 50-55 dBZ were generated in the spiral bands of Floyd, and then dissipated upon crossing the frontal boundary. Based on the degree of instability aloft (Fig. 4.17), and the dropsonde data, the following may explain the diminished cellular echo intensity. As stated by Bryan and Fritsch (2000) ascent in the presence of moist absolute instability reduces the temperature difference between parcels and their environment. Mesoscale low-level slab ascent occurred over the coastal front as a result of the strong deep layer flow normal to the boundary (Fig. 4.19). The atmosphere surrounding the parcels above the frontal boundary warmed, due to increased amounts of θ_e, thus decreasing parcel buoyancy.

It is believed the contiguous 20-45 dBZ echoes along and west of the frontal boundary were maintained by the secondary frontal circulation with the addition of hydrometeors that, on a Lagrangian time, took time to fall out of the decaying 50-55 dBZ cells. Furthermore, the persistent region of solid radar echoes immediately along and west of the front is consistent with the theory of slab ascent as presented by Bryan and Fritsch (2000).

The radar echoes produced by Floyd deteriorated and became increasingly disorganized as the hurricane moved closer to Cape Fear. At 2146, the eye of Floyd (not shown) became visible in the LTX radar imagery. East and south of the eyewall, precipitation echoes were sporadic, possibly due to radar attenuation and/or the effect of the mid-level dry air observed on satellite as it was wrapped from the southwest into the hurricane center. However, echoes proximate to the eyewall in northern and western

sections maintained a discernible symmetry. As Floyd tracked northward towards North Carolina, the eye traveled immediately along and east of the frontal precipitation band.

By 0200 radar imagery indicated that the frontal precipitation band was wrapping into the west and southwestern eyewall sides as the boundary traveled eastward and arched in toward Floyd's eye (Fig. 4.25). The eastward movement on radar was constant with the frontal motion observed by the MMs in the eyewall. The "bowing" in the reflectivity imagery continued as the center of the hurricane traveled north into Virginia. At 0430, the increasingly ragged eye began to fill with 10-15 dBZ echoes while its horizontal diameter contracted. The eye filled completely and became asymmetrical in shape by 0530. This trend continued through the time of landfall at 0630 (Fig. 4.26). Remote sensors indicated that Floyd had weakened prior to landfall and were consistent with aircraft reconnaissance reports. Reconnaissance reported a 4-mb rise in Floyd's minimum central pressure between 0300 and 0600 (Fig. 4.27). As the storm advanced northward over North Carolina, all precipitation behind the hurricane ceased.

Radar-derived storm total precipitation amounts greater than 38 cm were estimated by the LTX radar. For the period of 1329, 15 September to 1039, 16 September, LTX radar estimated storm total precipitation yielded amounts greater than 22 cm (Fig. 4.28). The primary axis of precipitation was oriented NNE-SSW with a precipitation maximum aligned along and immediately west of the mean frontal boundary position.

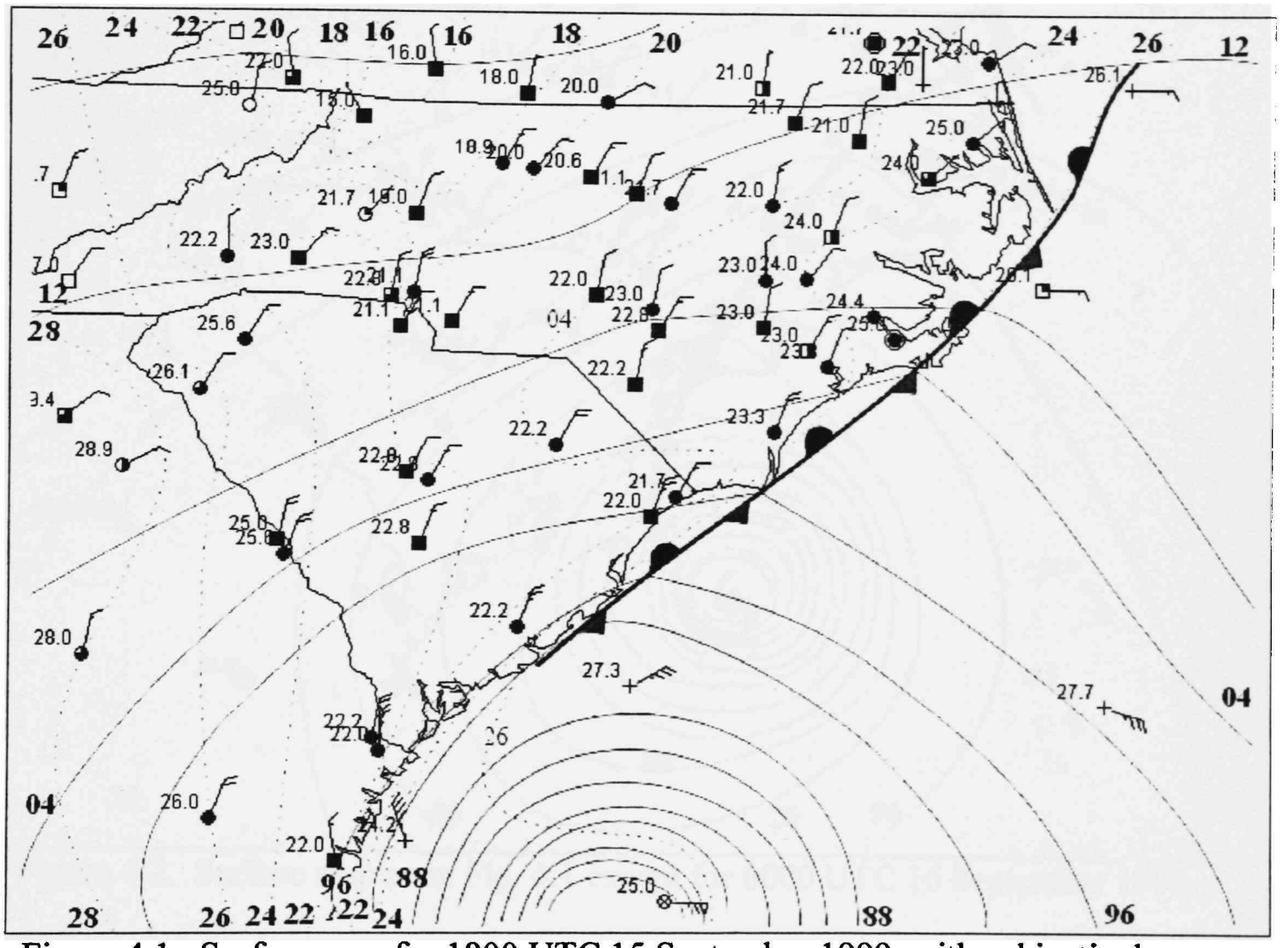

Figure 4.1. Surface map for 1800 UTC 15 September 1999, with subjectively analyzed mean sea level isobars (solid) every 4 mb (labeled every other isobar to 988 mb), and isotherms (dashed) every 2°C (labeled every isotherm). Shaded region represents surface pressure falls ≥4 mb 3 hr^{-1}. Standard station model in abbreviated format; temperature in tenths °C and sky conditions reported. Winds in knots with one pennant, one full barb, and one half barb equal to 50, 10, and 5 knots, respectively.

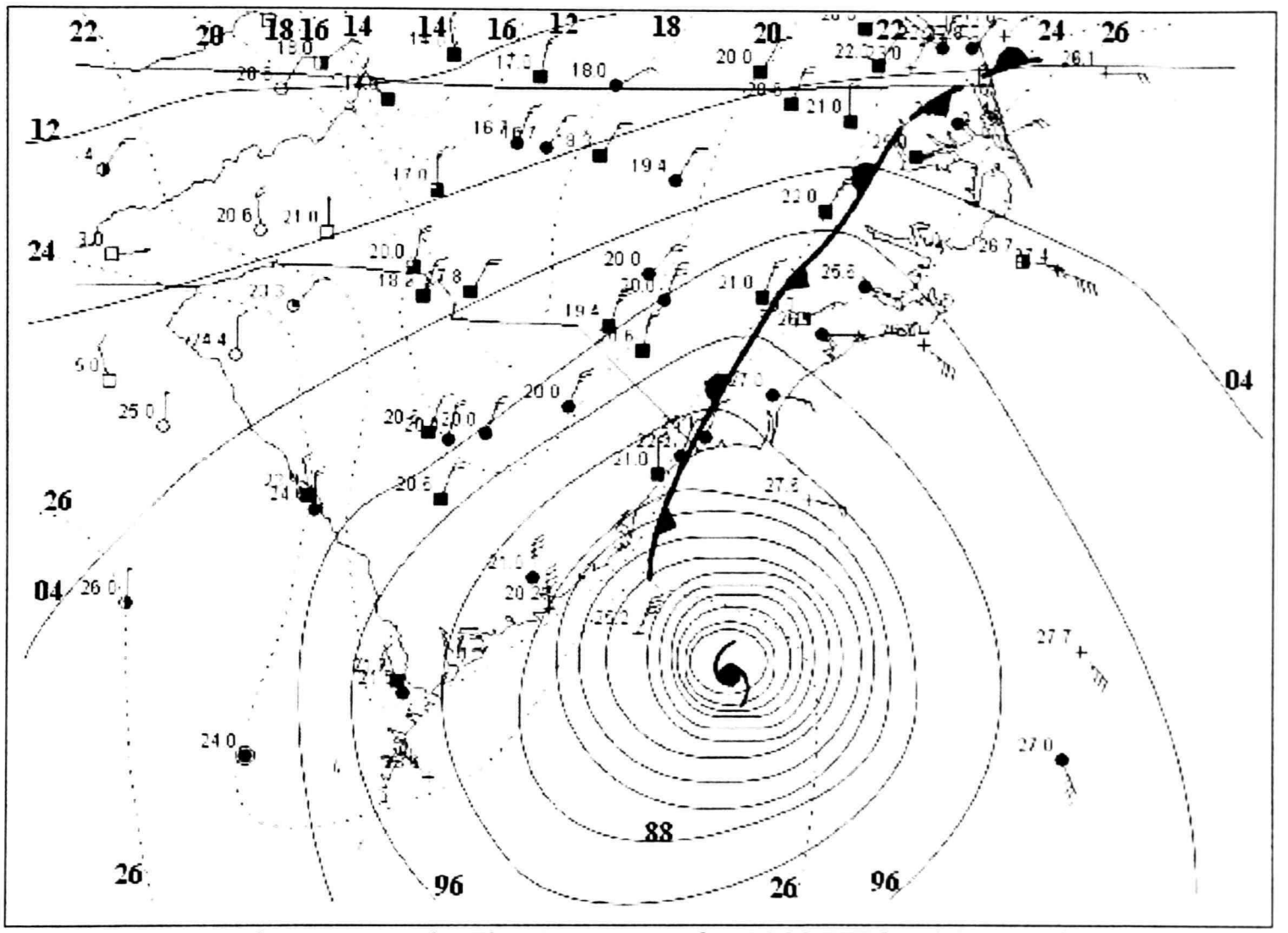

Figure 4.2. Surface map as in Fig. 4.1 except for 0000 UTC 16 September 1999.

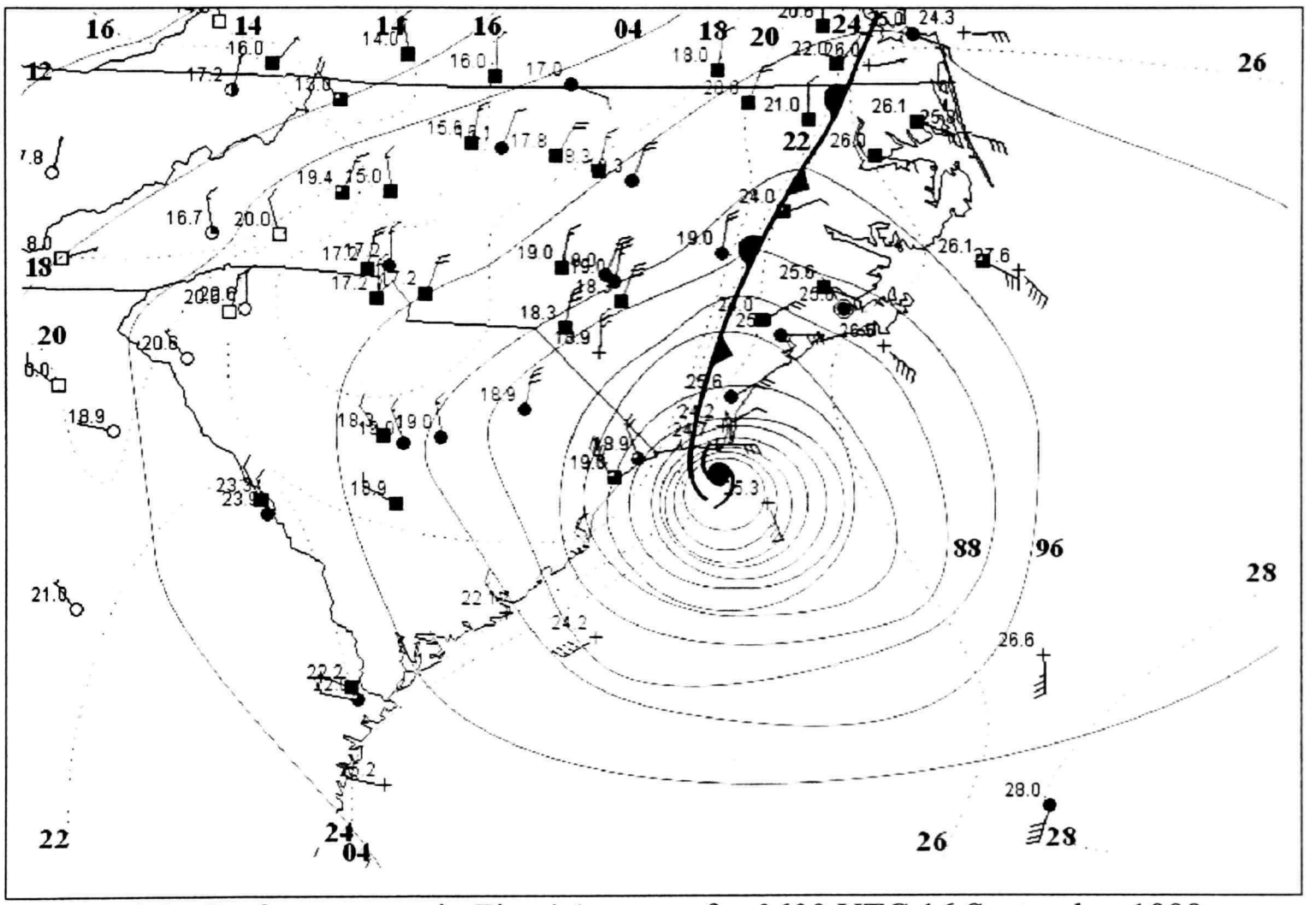

Figure 4.3. Surface map as in Fig. 4.1 except for 0600 UTC 16 September 1999.

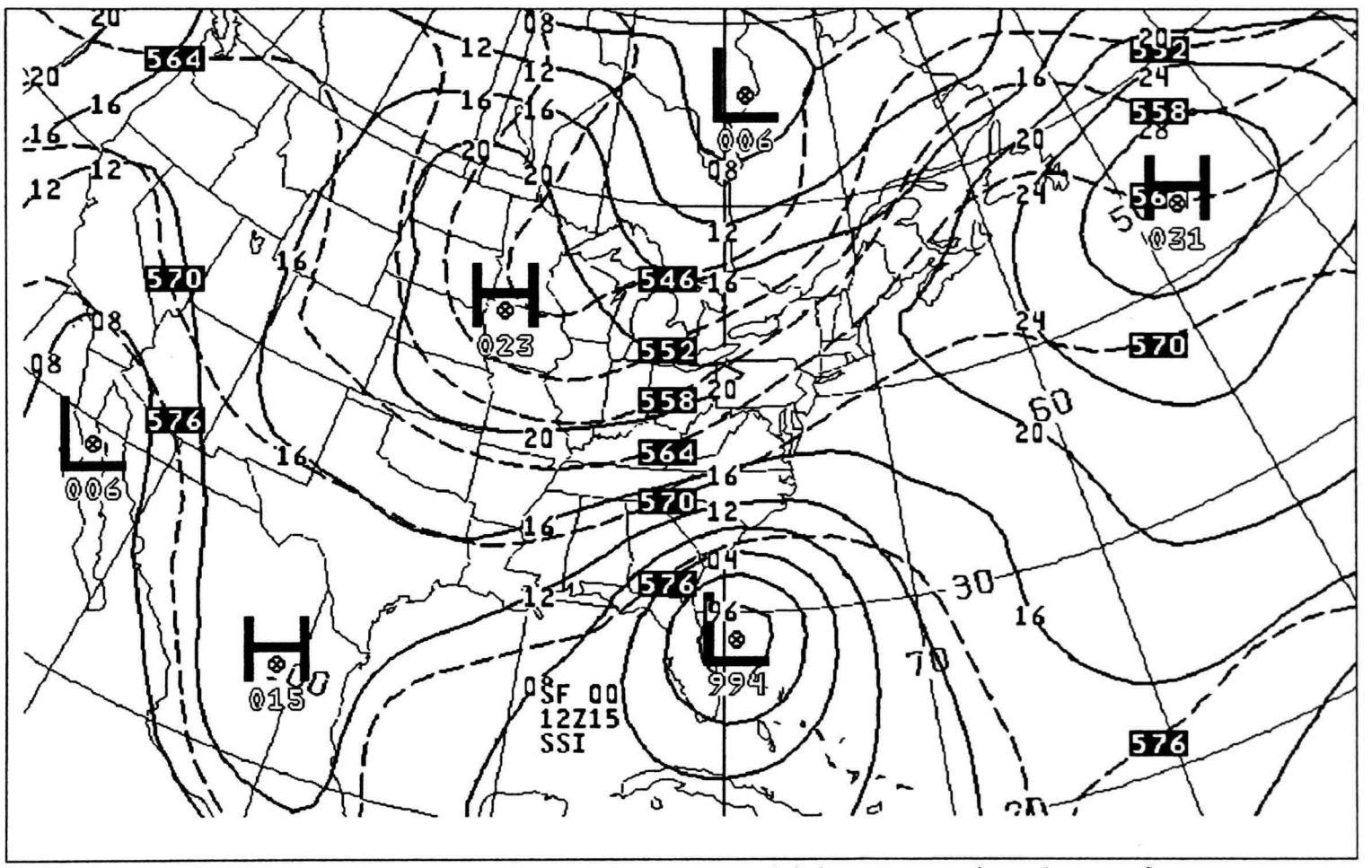

Figure 4.4. Surface pressure and 1000-500 mb thickness sectional map for 1200 UTC 15 September 1999.

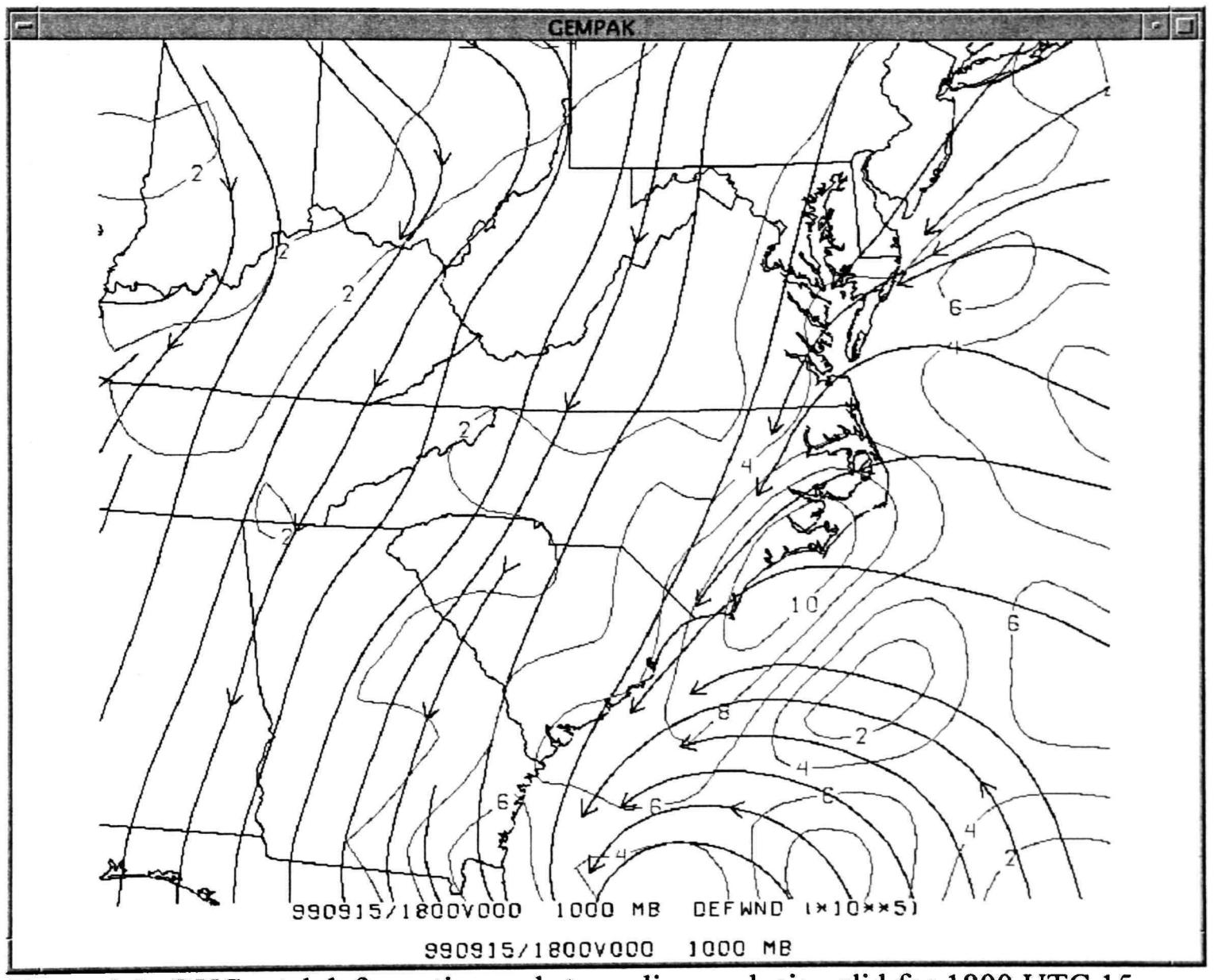

Figure 4.5. RUC total deformation and streamline analysis valid for 1800 UTC 15 September 1999. Deformation contoured every 2 x 10^{-5} s^{-1}.

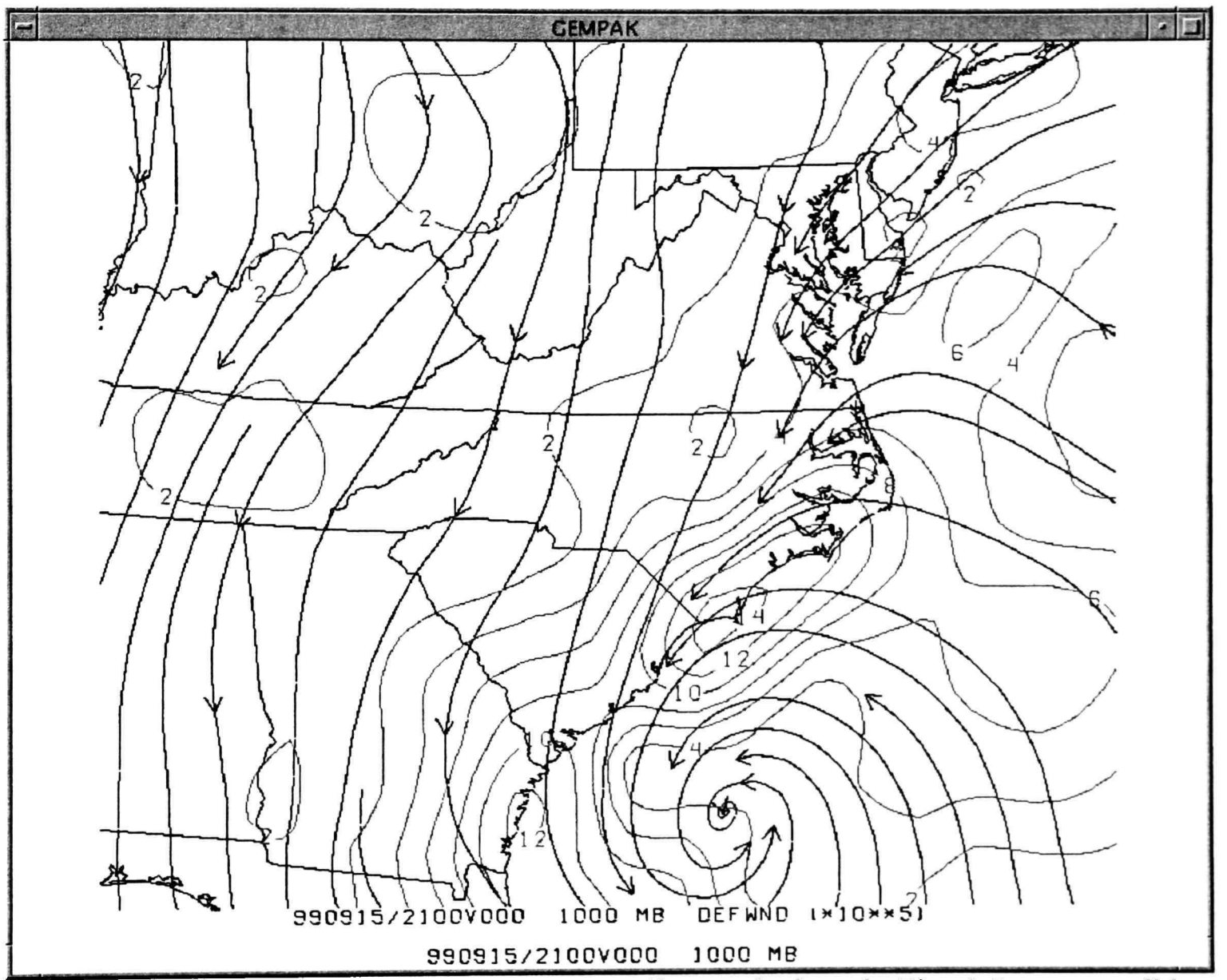

Figure 4.6. RUC total deformation and streamline analysis as in Fig. 4.5 except valid for 2100 UTC 15 September 1999.

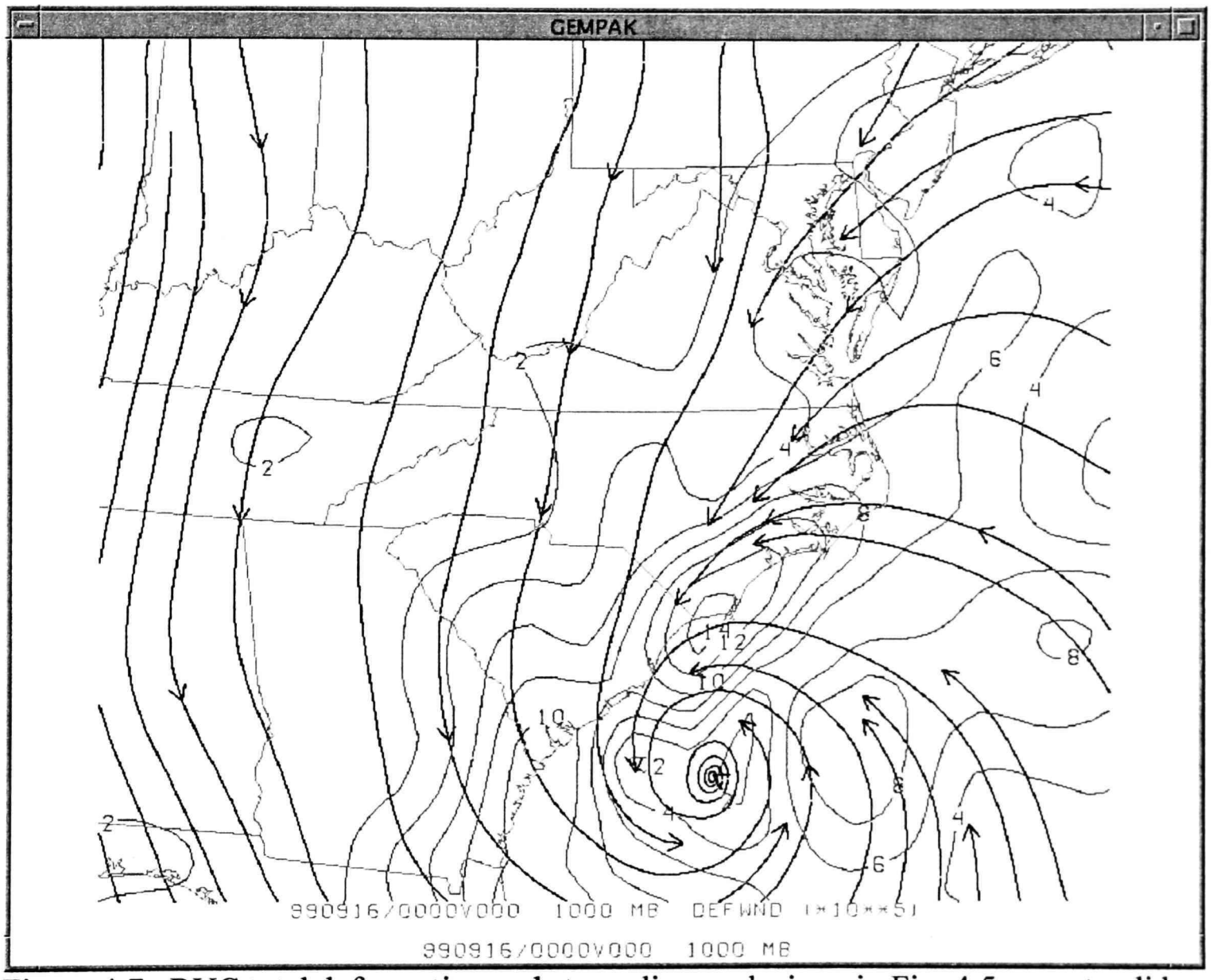

Figure 4.7. RUC total deformation and streamline analysis as in Fig. 4.5 except valid for 0000 UTC 16 September 1999.

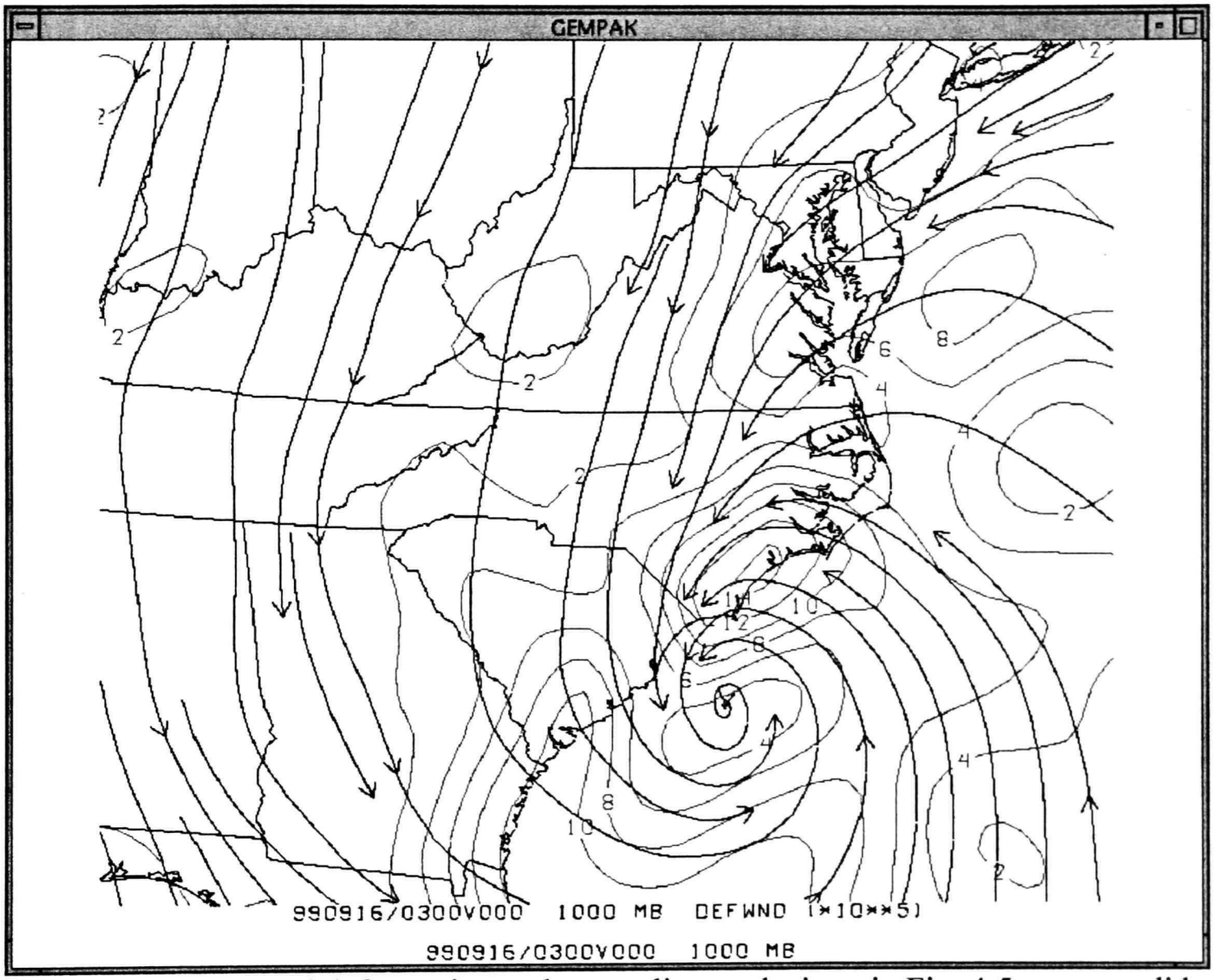

Figure 4.8. RUC total deformation and streamline analysis as in Fig. 4.5 except valid for 0300 UTC 16 September 1999.

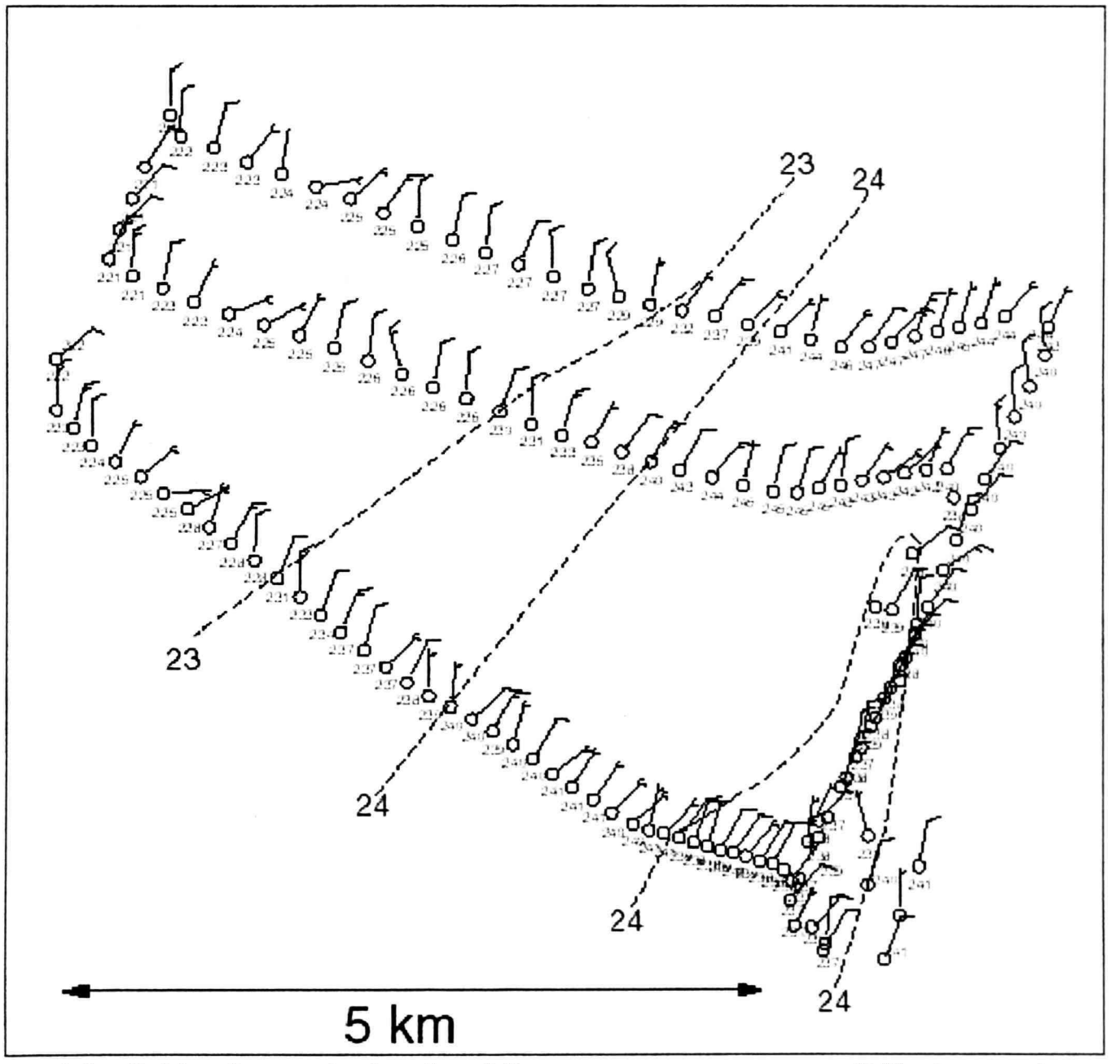

Figure 4.9. Subjective analysis of mobile mesonet temperature (°C) observations across the coastal front near North Myrtle Beach, SC, at 0131-0201 UTC on 16 September 1999. Observations are 18-sec averages (3 observations) plotted every 30 sec using time-to-space conversion with a motion vector from 190 at 8.0 m s^{-1}. Temperature and wind as in Fig. 4.1. Isotherms (dashed) every 2°C.

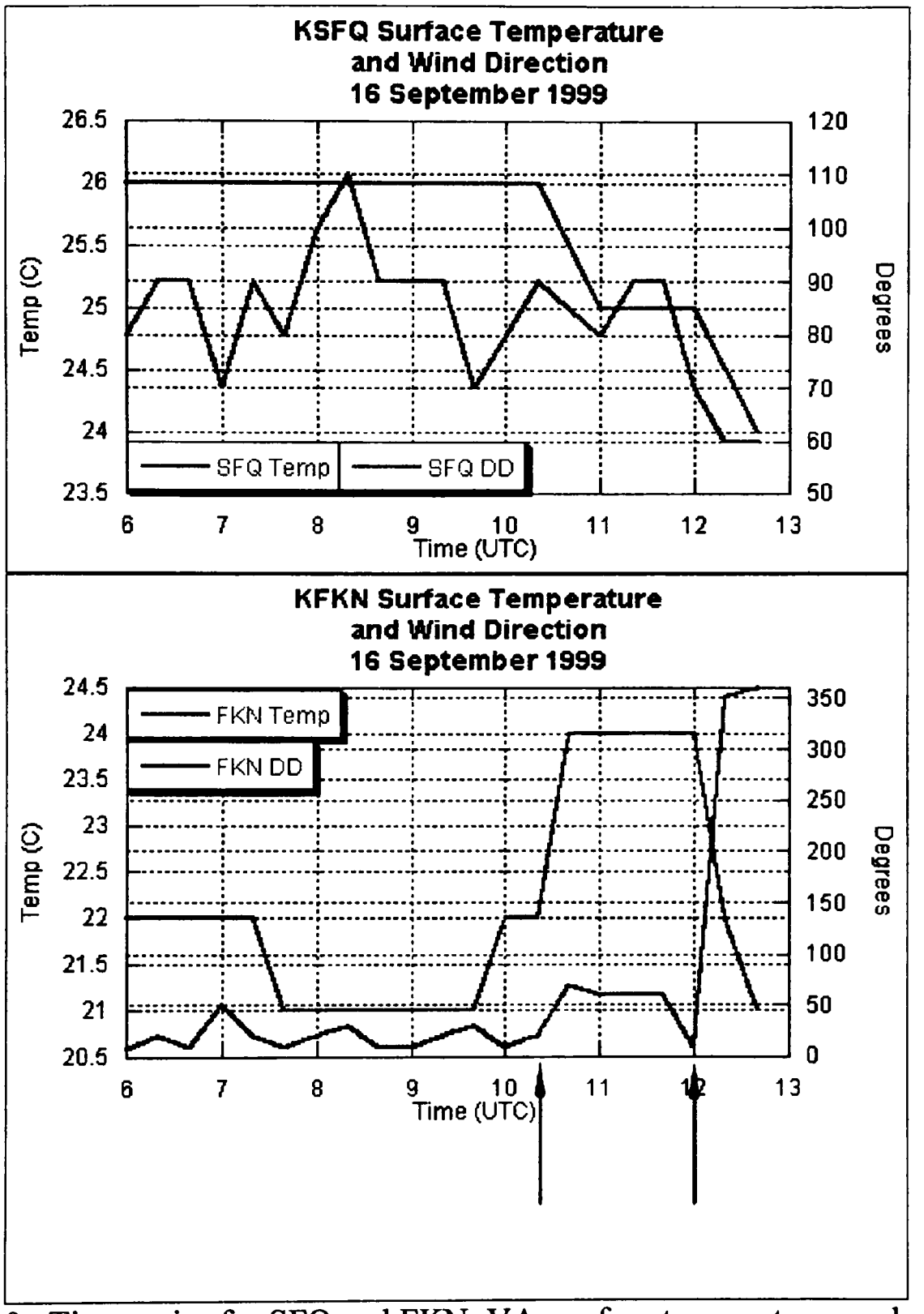

Figure 4.10. Time series for SFQ and FKN, VA, surface temperatures and wind directions for the time between 0600-1240 UTC 16 September 1999. FKN is ~27 km due west of SFQ. The two arrows represent the times of FROPA at FKN. Note between 1020-1040 the coastal front moved west of the station with a 2°C increase in temperature and a 50° veering in winds. Between 1200-1220 the coastal moved east of the station with a 2°C drop in temperature during a pronounced backing of the winds.

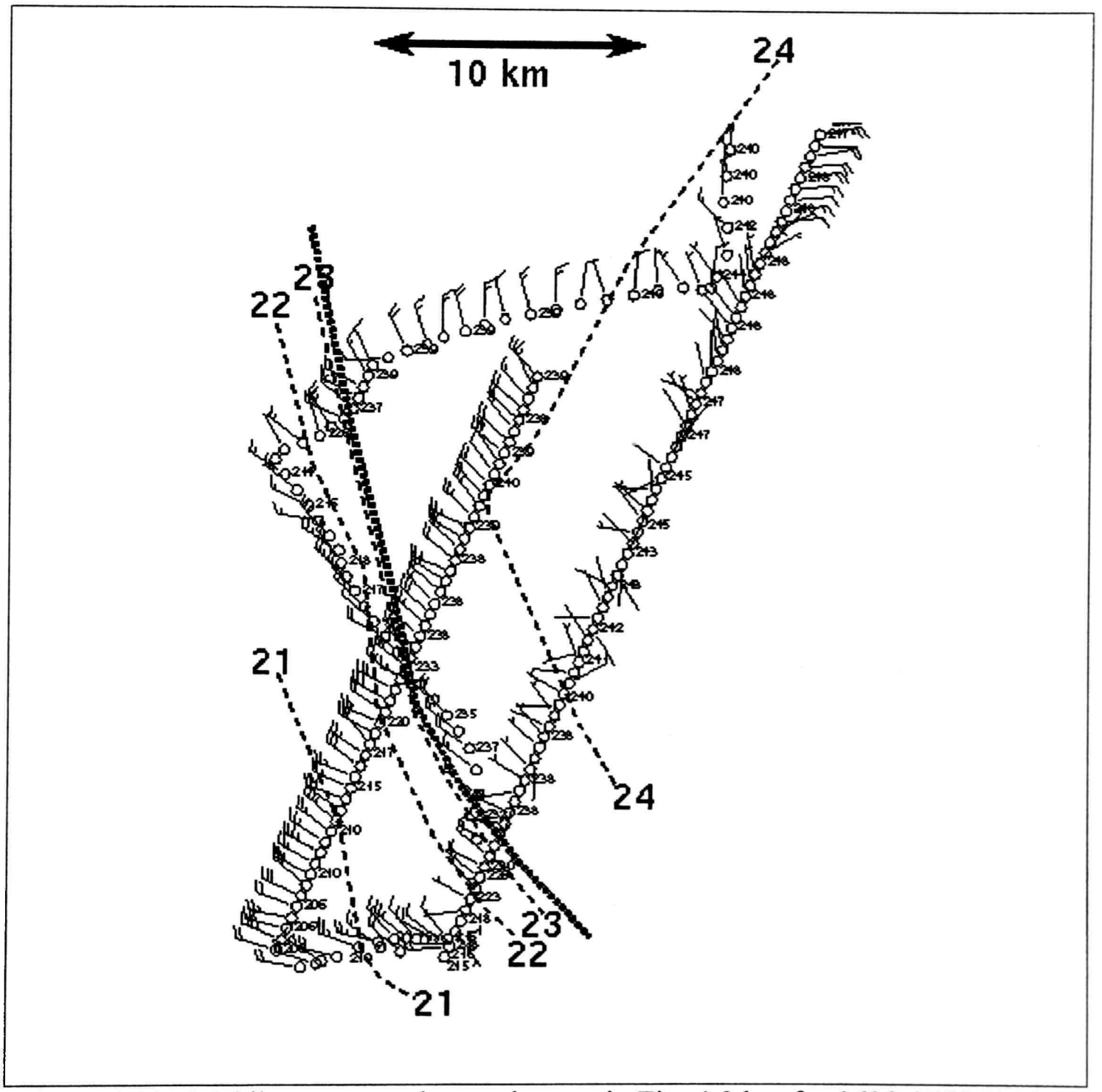

Figure 4.11. Mobile mesonet observations as in Fig. 4.9 but for 0628-0750 UTC near Southport, NC, 16 September 1999. Mobile mesonet data plotted every 60 sec using time-to-space conversion with a motion vector from 190 at 9.25 m s^{-1}. Approximate frontal location marked with the bold line.

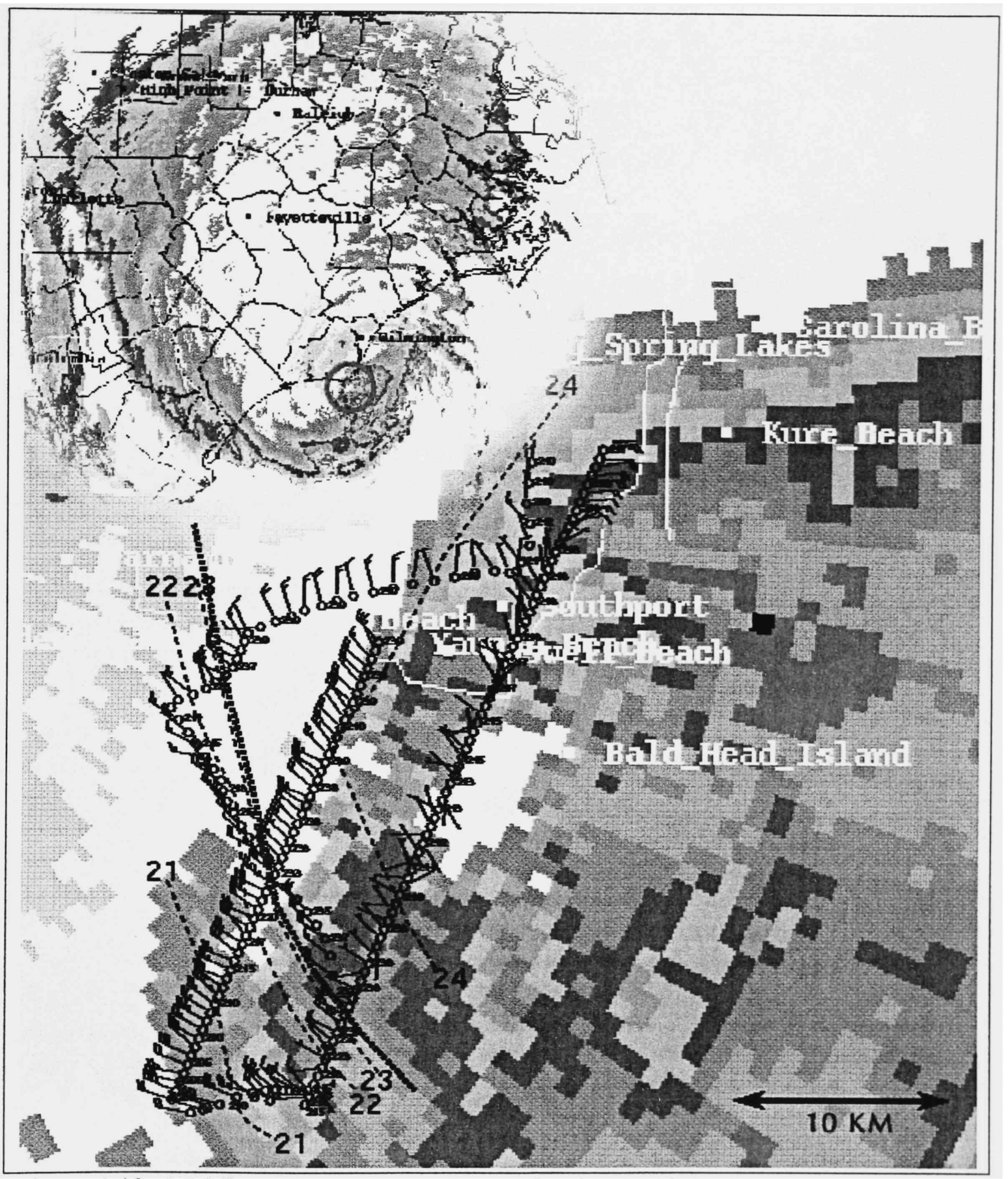

Figure 4.12. Mobile mesonet observations as in Fig. 4.11 but overlaid with KLTX base reflectivity for 0628 UTC. The red ring in the radar inset represents the region blown up. The radar image has been scaled to size.

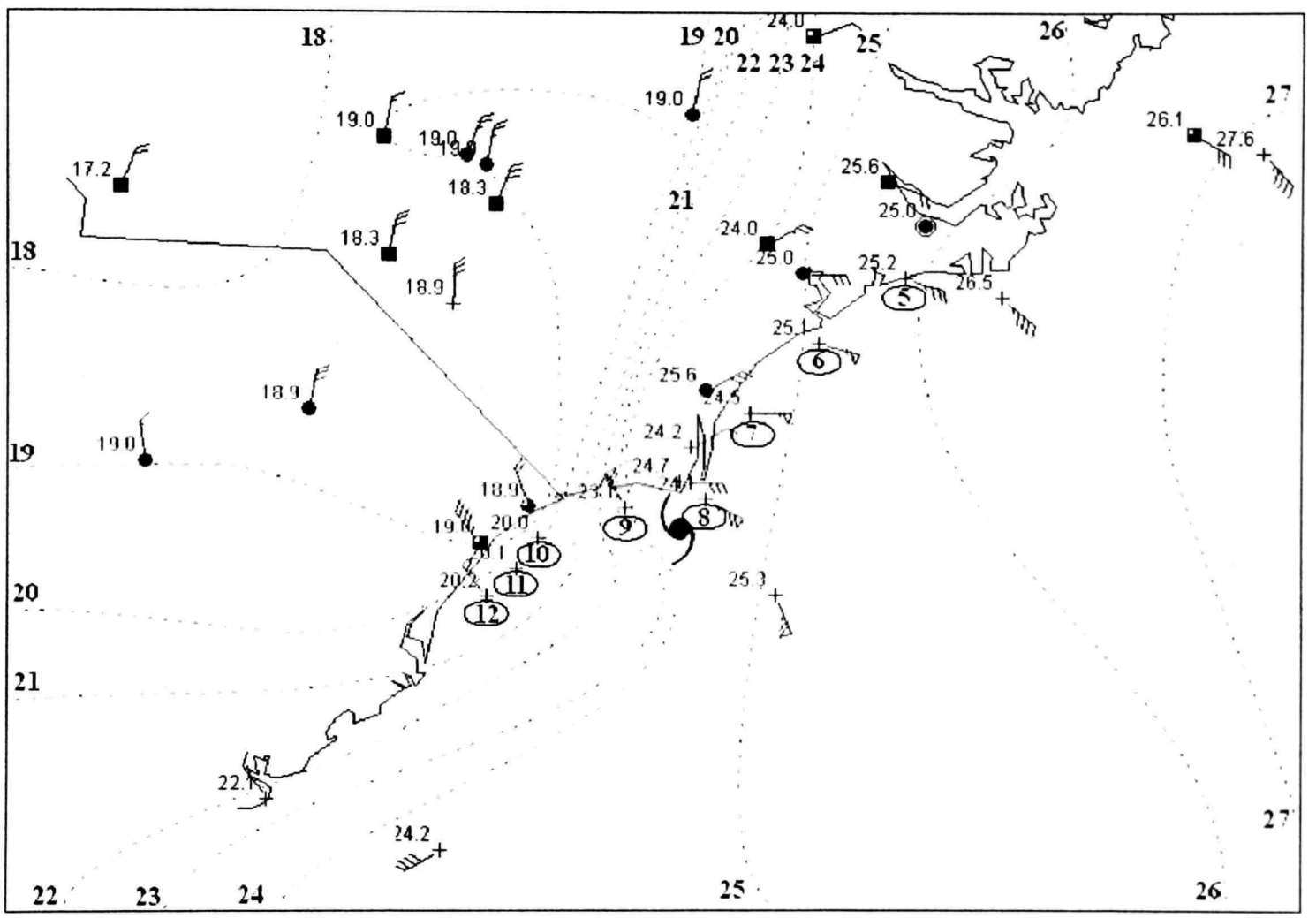

Figure 4.13. Surface map for 0600 UTC 16 September 1999, with subjectively analyzed isotherms (dashed) every 1°C (labeled every isotherm). Standard station model as in Fig. 4.1. Dropsonde data has been incorporated into the map using the last reported observation before splash point. Dropsonde ID enclosed by oval.

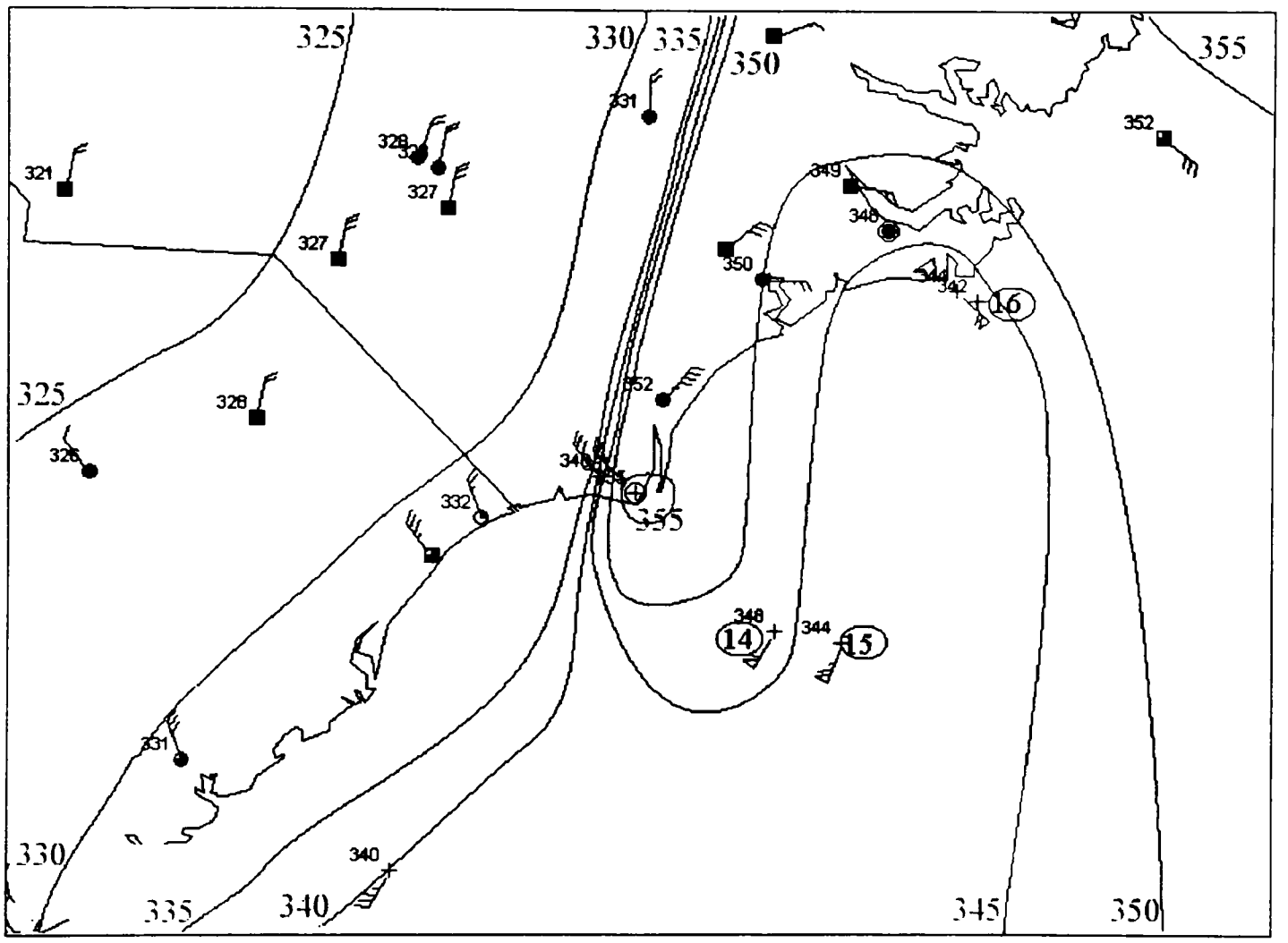

Figure. 4.14. Surface map as in Fig. 4.13 except for 0700 UTC 16 September 1999 with equivalent potential temperature contoured every 5K.

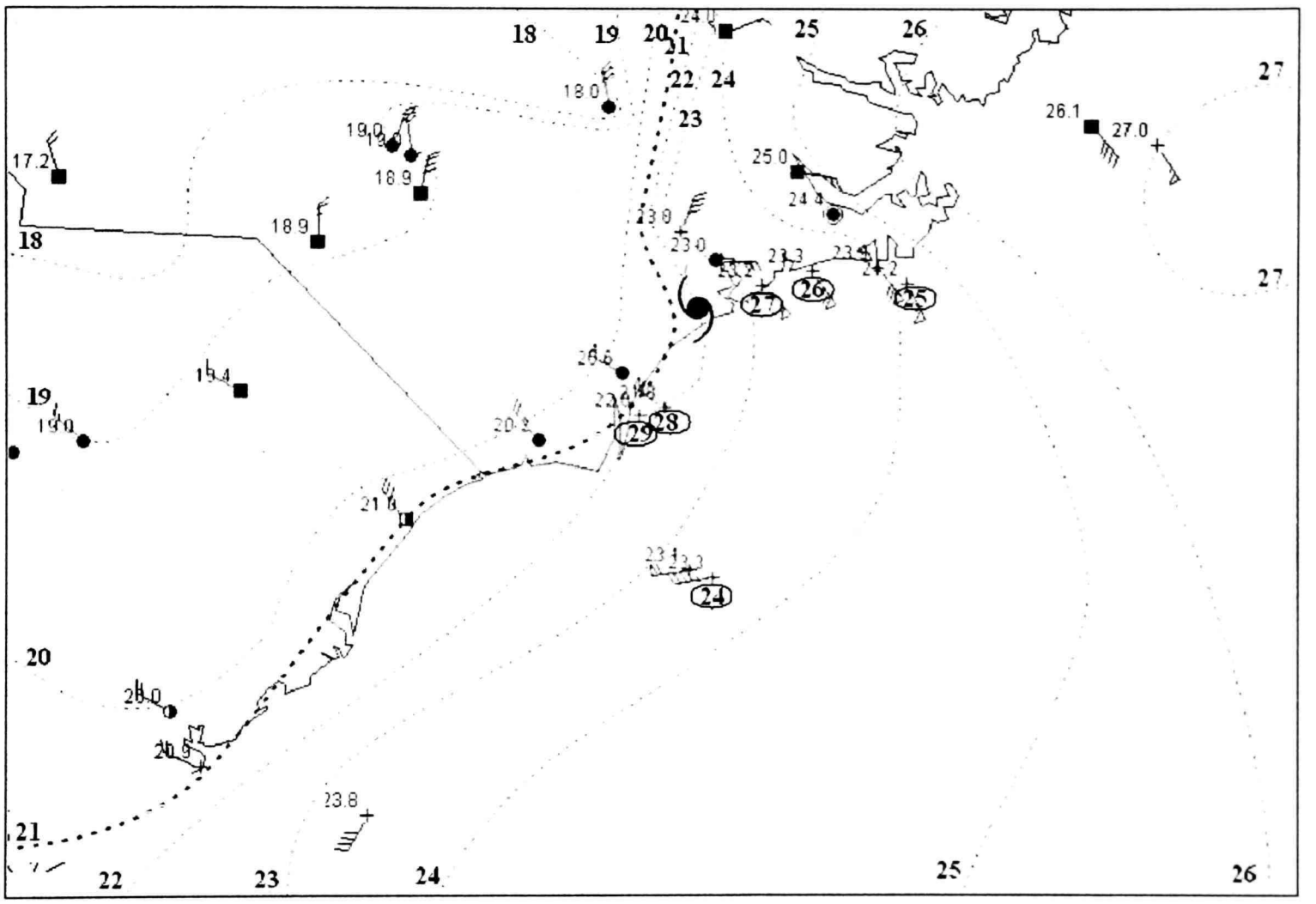

Figure. 4.15. Surface map as in Fig. 4.13 but for the time 0900 UTC 16 September 1999. Note the contracted baroclinic zone north of the hurricane's center.

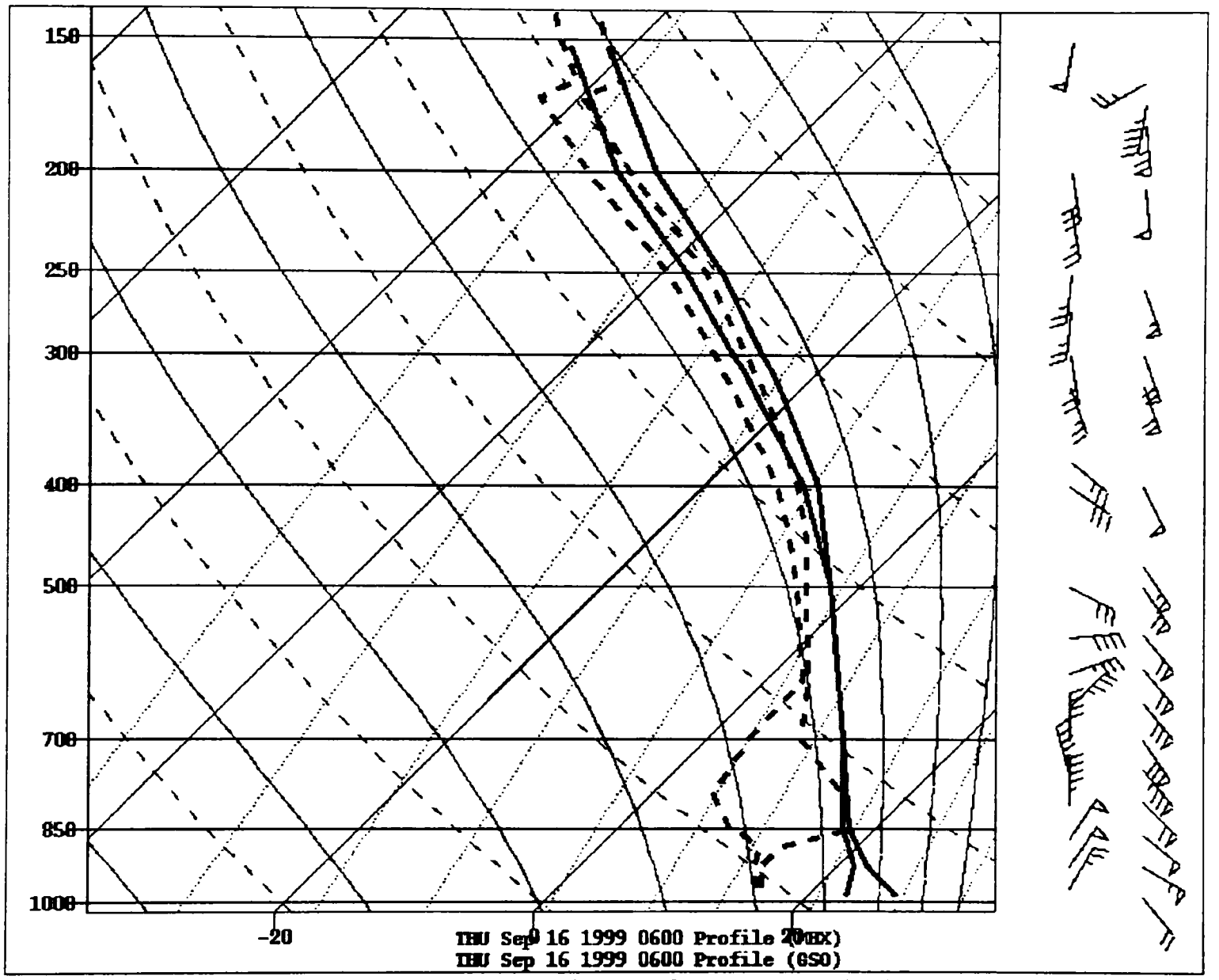

Figure 4.16. Sounding in skew *T*-log *p* format for GSO (dashed) and MHX (solid) for 0600 UTC 16 September 1999. Winds as in Fig. 4.1. MHX winds are farthest right.

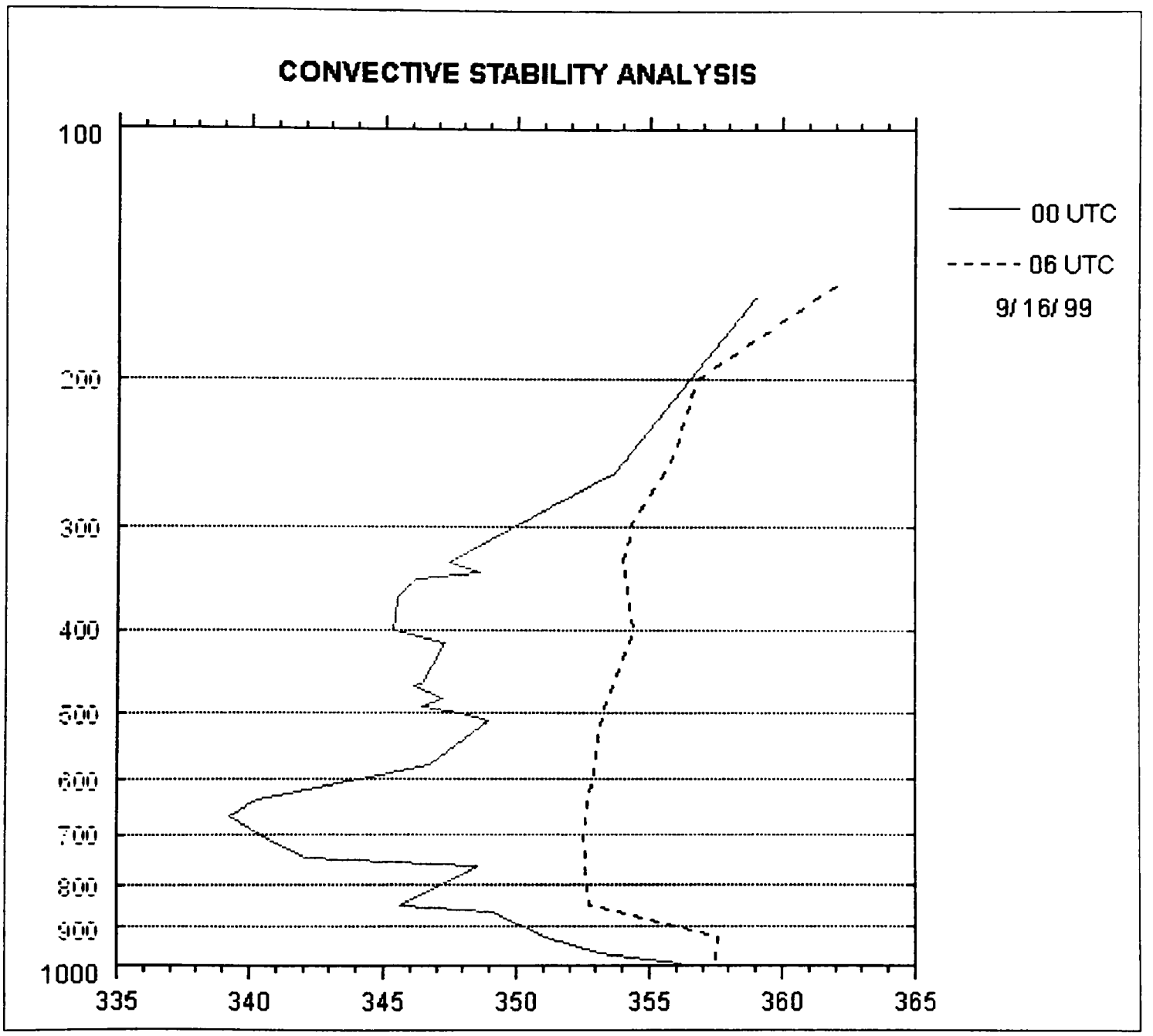

Figure 4.17. 0000 UTC (solid) and 0600 UTC (dashed) 16 September convective stability analysis for Morehead City (MHX), NC. Abscissa is θ_e (K); ordinate is pressure (hPa).

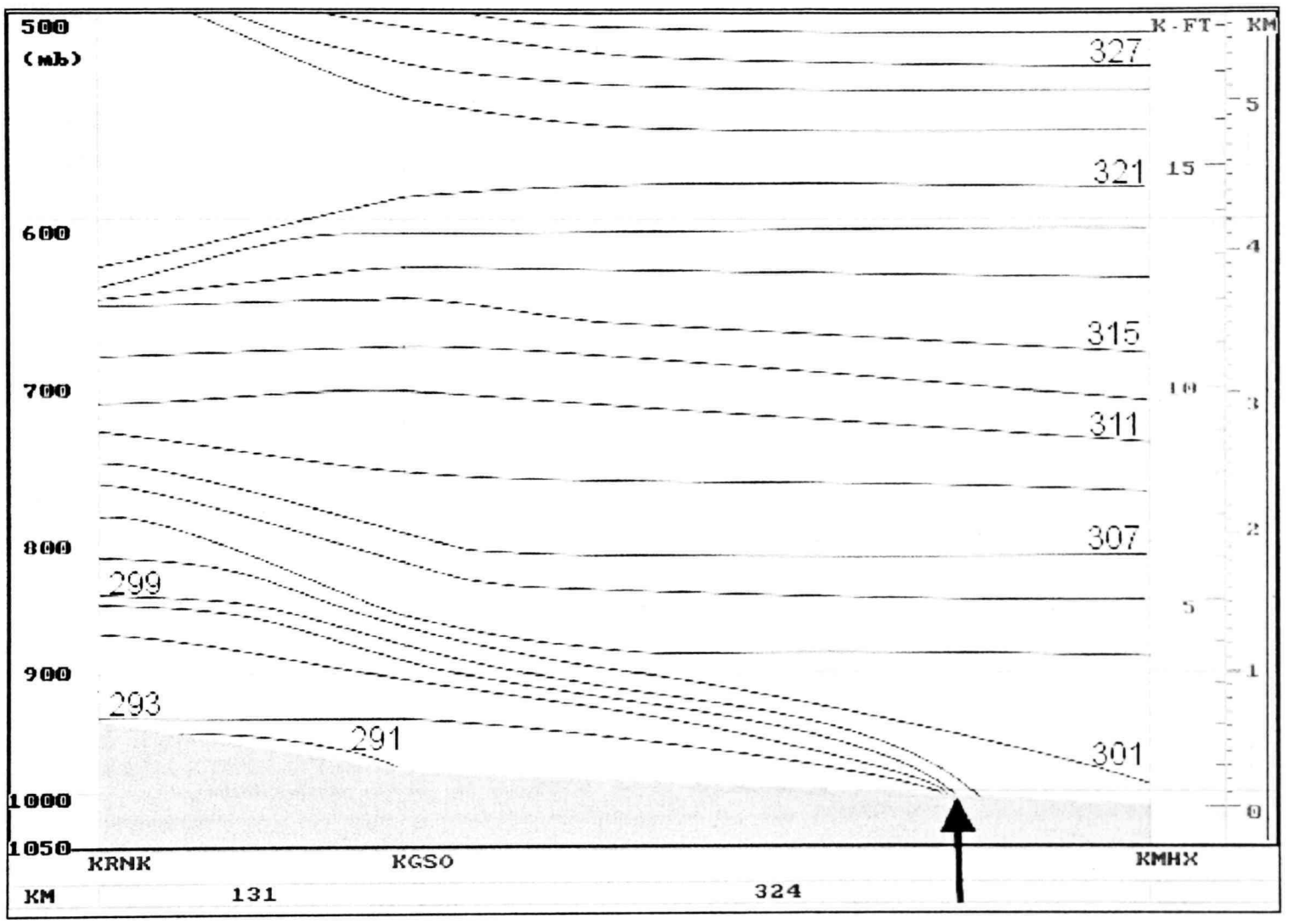

Figure 4.18. An east-west subjectively analyzed cross section of potential temperature (solid, 2K internals) between Morehead City, NC, Greensboro, NC, and Roanoke, VA, on 0600 UTC 16 September 1999. Black arrow denotes 0600 UTC frontal boundary position. The kilometer scale along the bottom of the figure is distance separation between the soundings.

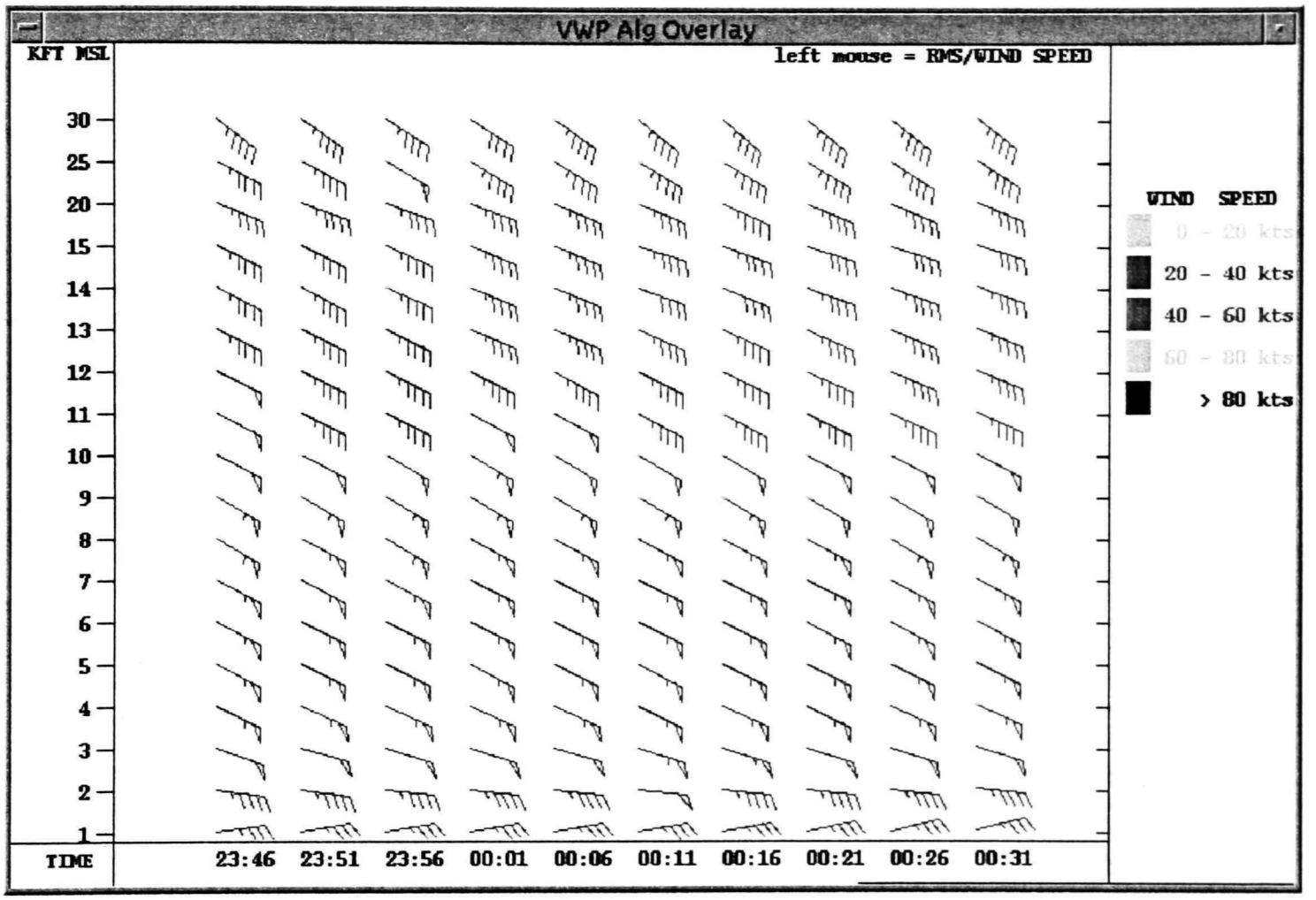

Figure 4.19. LTX WSR-88D VAD depicting wind profiles 2346-0031 UTC 16 September 1999. Winds as in Fig. 4.1. The coastal front was ~ 15 km west of this location.

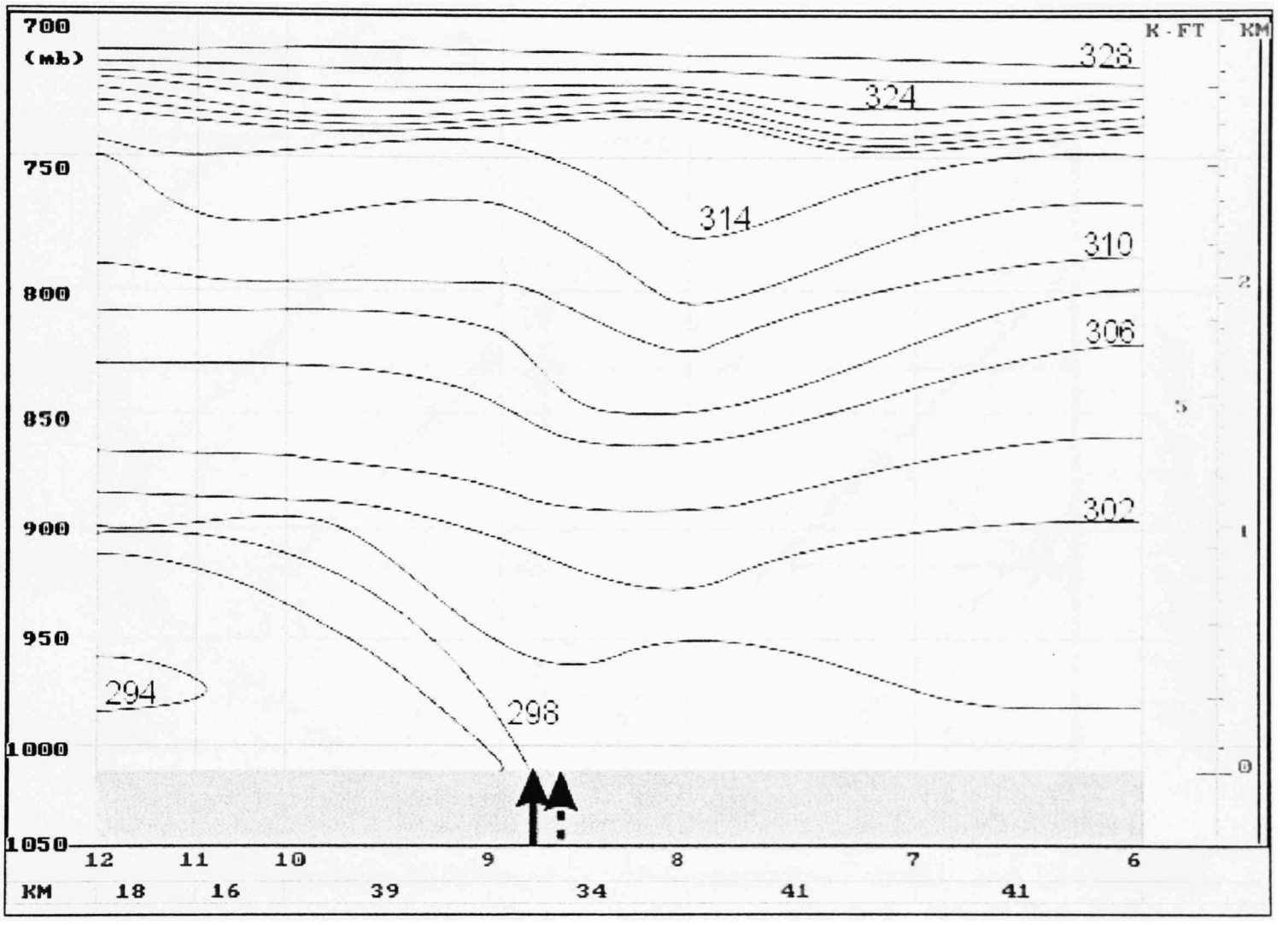

Figure 4.20. Cross section of potential temperature as in Fig. 4.18 except for dropsondes 6-12 released between 0539-0614 UTC 16 September 1999. Dropsonde horizontal positions are shown in Fig. 3.1. The solid (dashed) black arrow denotes 0600 UTC frontal boundary (hurricane) position. The center of Floyd is 21 km south-southwest of sonde 8 and 29 km south-southeast of sonde 9.

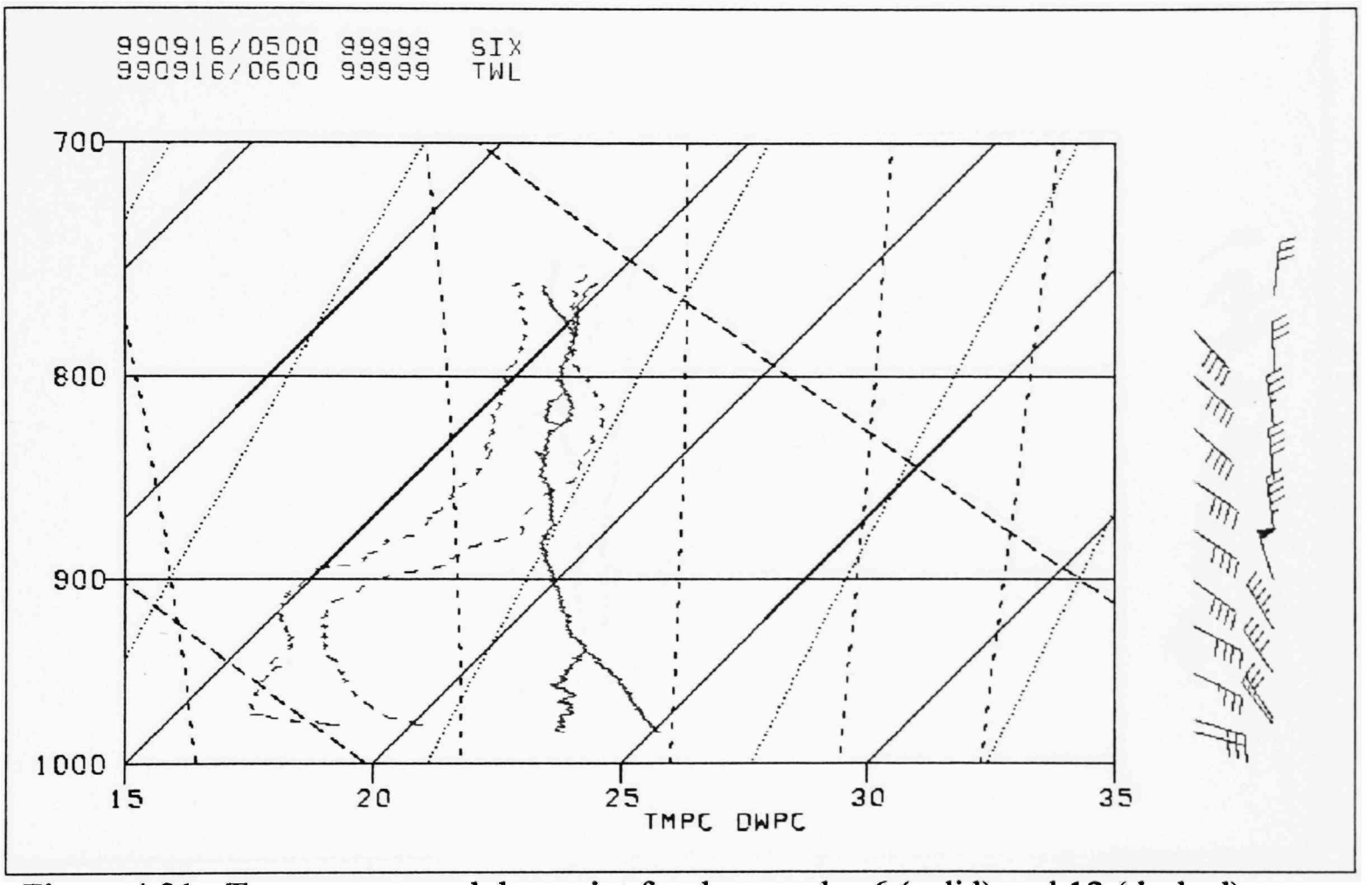

Figure 4.21. Temperature and dewpoint for dropsondes 6 (solid) and 12 (dashed). Data has been truncated above 750 mb. Winds as in Fig. 4.1. Wind data from dropsonde 12 are farthest right.

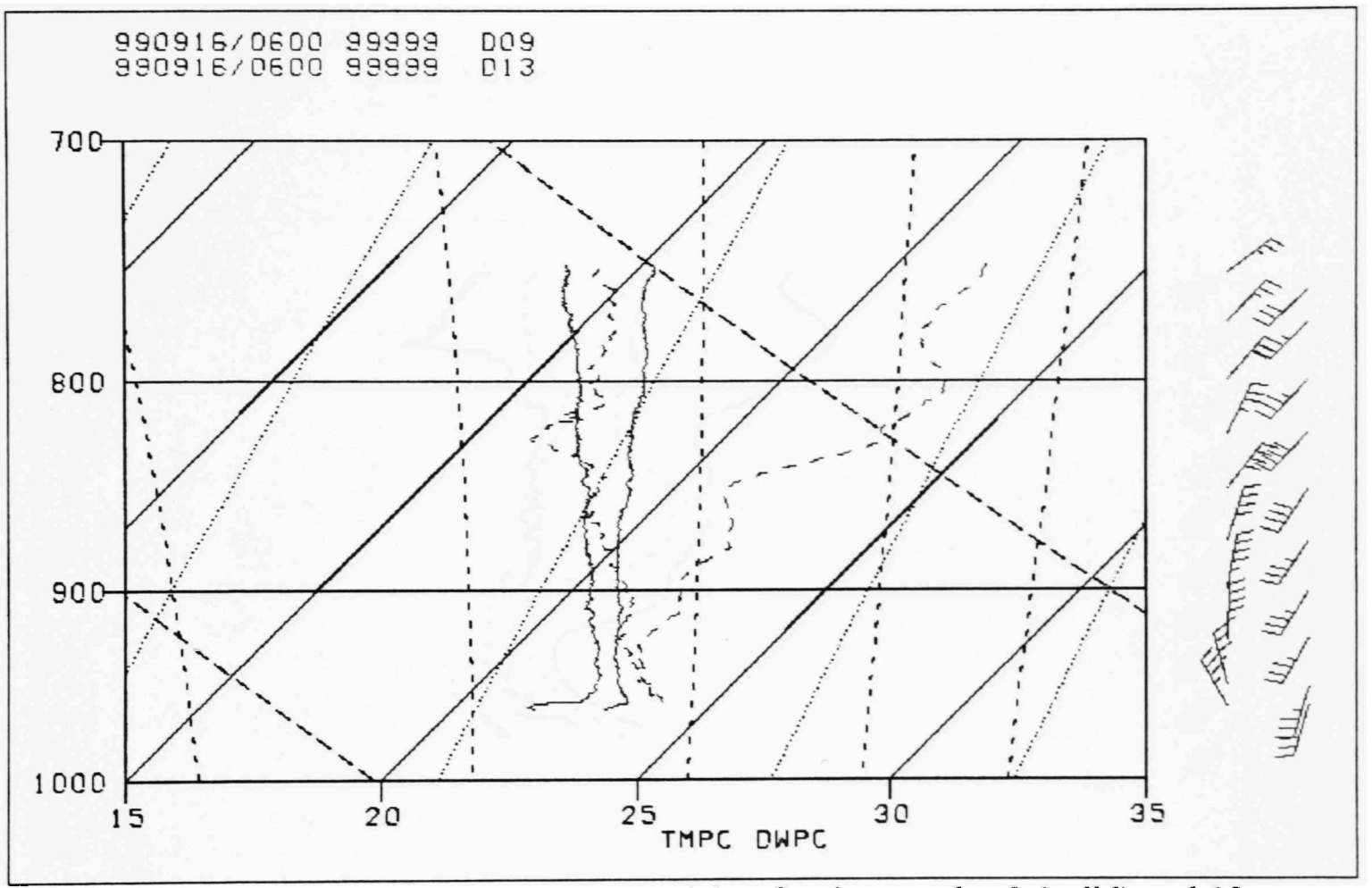

Figure 4.22. Dropsonde data as in Fig. 4.21 but for dropsondes 9 (solid) and 13 dashed. Wind data from dropsonde 13 are farthest right.

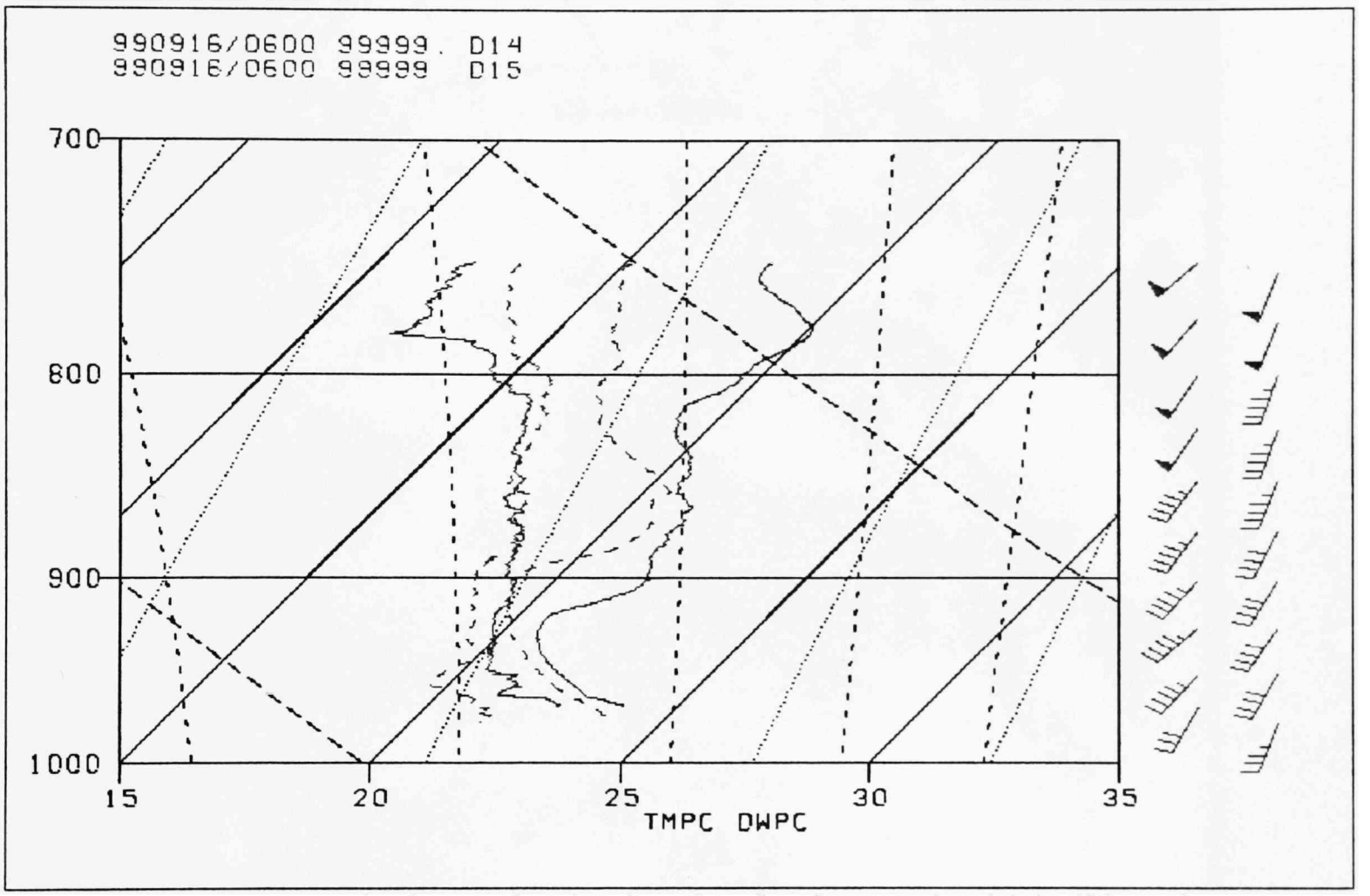

Figure 4.23. Dropsonde data as in Fig. 4.21 but for dropsondes 14 (solid) and 15 (dashed). Wind data from dropsonde 15 are farthest right.

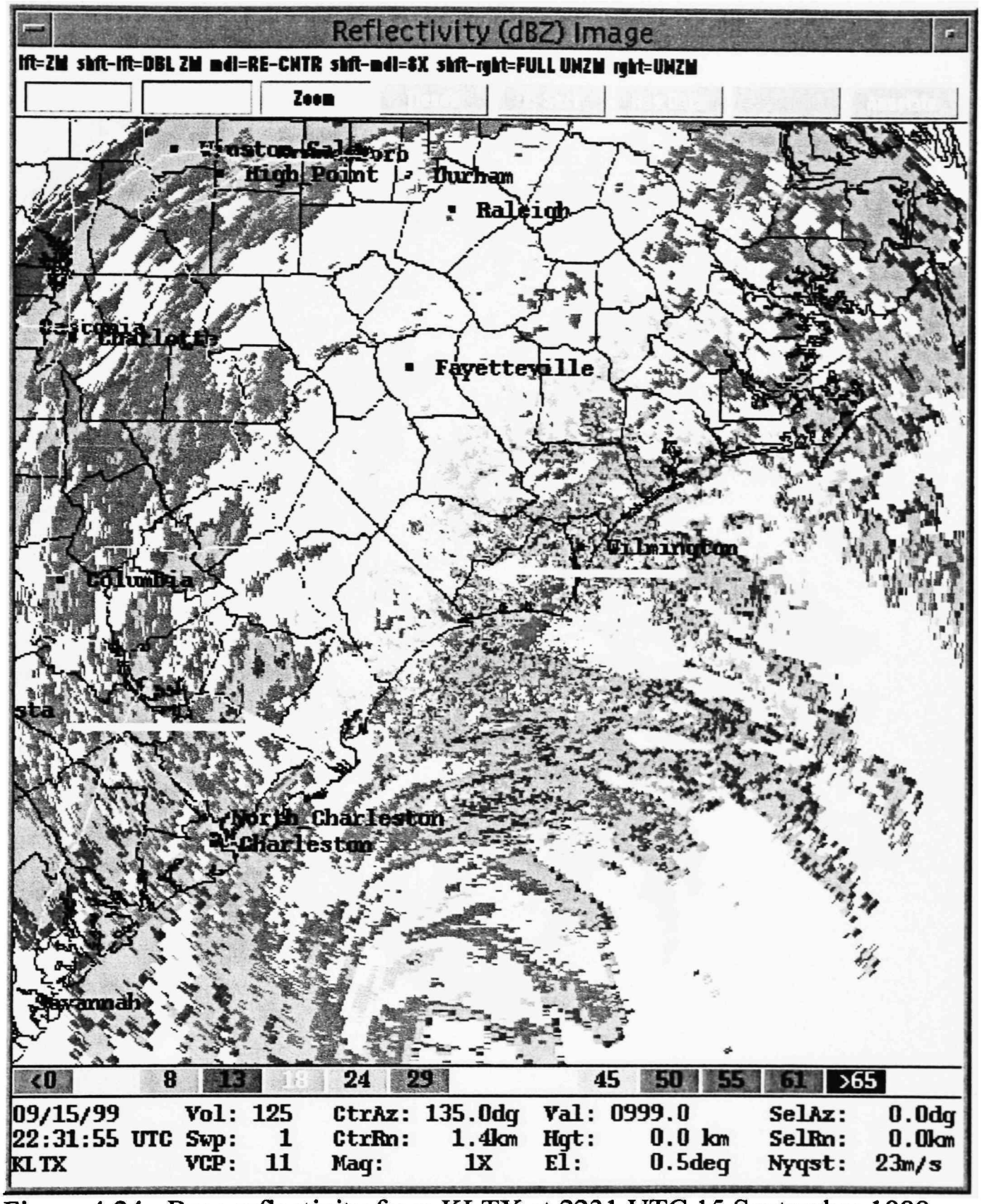

Figure 4.24. Base reflectivity from KLTX at 2231 UTC 15 September 1999. White arrows denote frontal precipitation band.

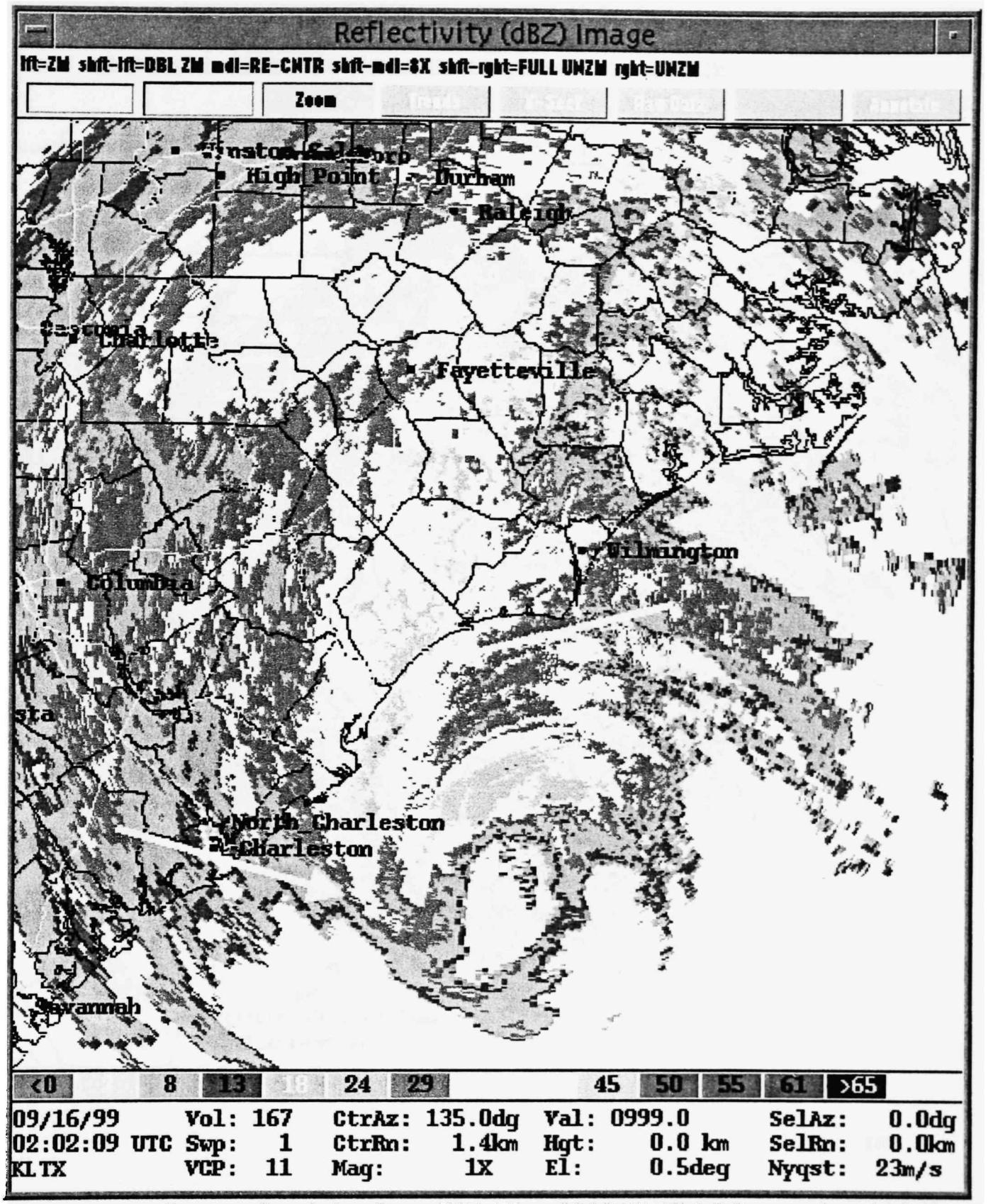

Figure 4.25. Base reflectivity from KLTX at 0202 UTC 16 September 1999. Note the bending of the frontal precipitation band into the southwest quadrant of the hurricane.

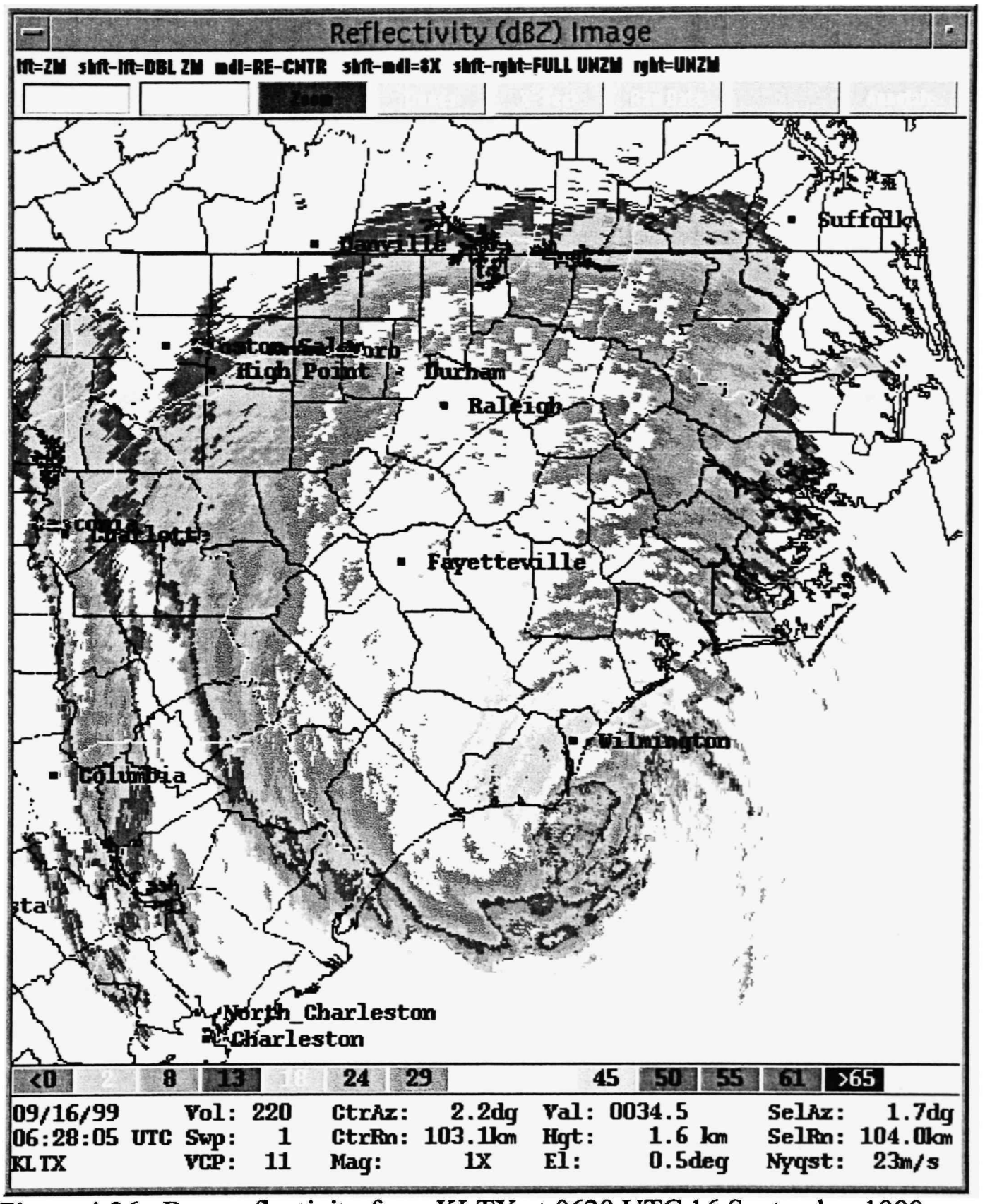

Figure 4.26. Base reflectivity from KLTX at 0628 UTC 16 September 1999.

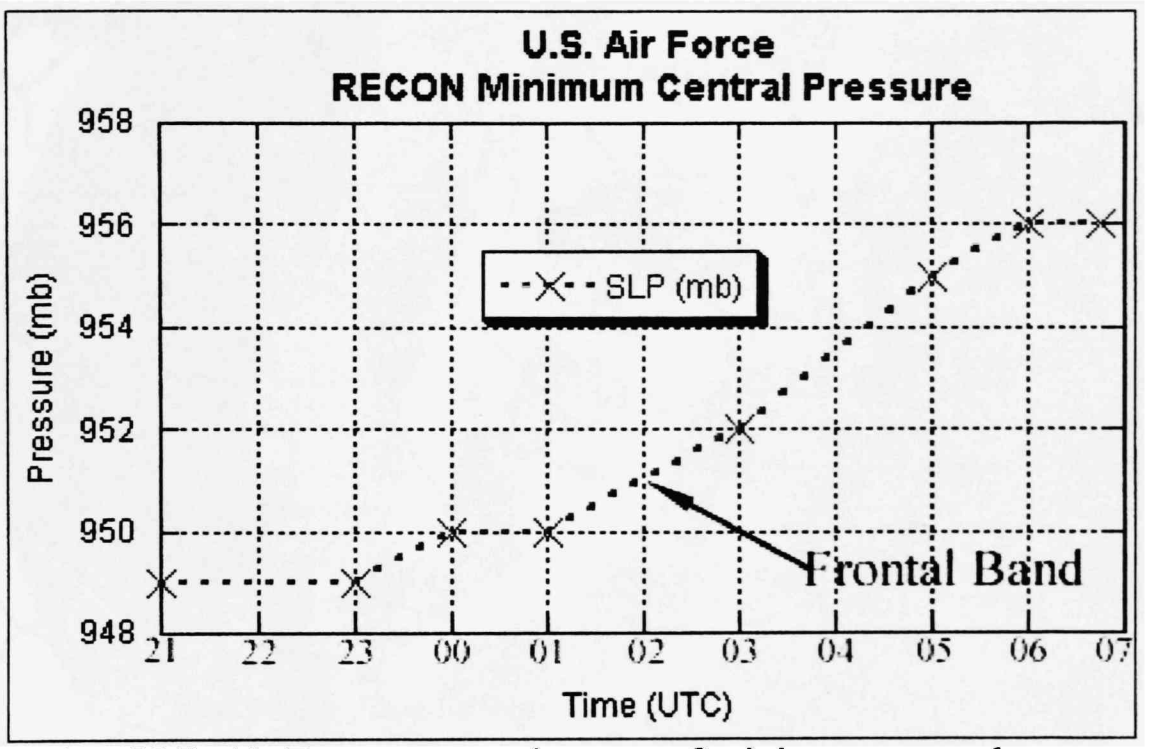

Figure 4.27. U.S. Air Force reconnaissance of minimum central pressure for the times 2100-0645 UTC 15-16 September 1999. Abscissa is time (UTC); ordinate is pressure (mb). Hash marks represent observations. Dotted line represents pressure trend. Arrow with text denotes the time the precipitation rain band was first observed on the LTX radar wrapping into Floyd's circulation.

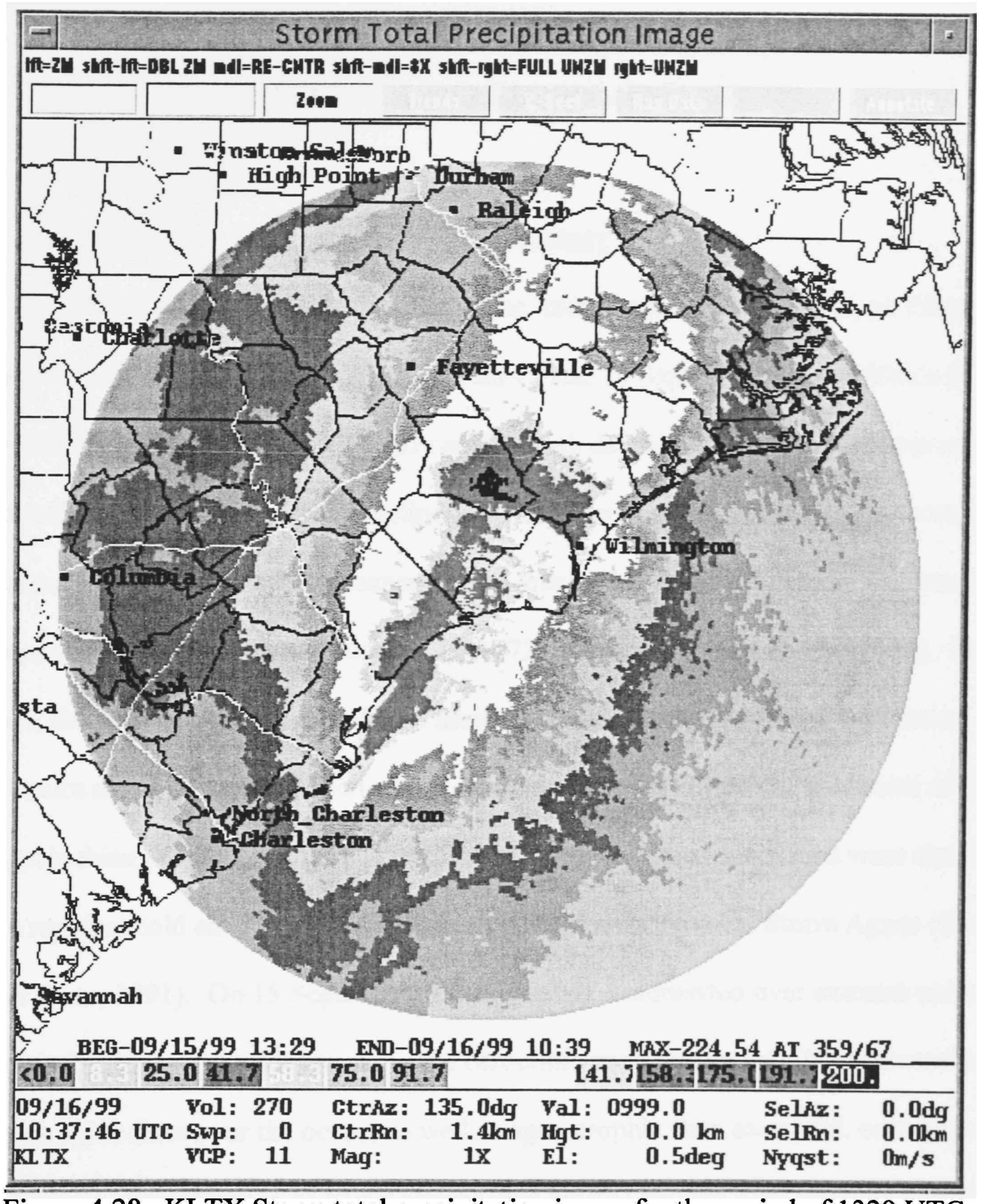

Figure 4.28. KLTX Storm total precipitation image for the period of 1329 UTC 15 September to 1039 UTC 16 September. Precipitation values in millimeters.

CHAPTER V

SUMMARY AND RECOMMENDATIONS

5.1 Summary

This thesis presents an analysis of the interaction between Hurricane Floyd and a coastal front prior to and during landfall on 15 and 16 September 1999. Within this period, a coastal front oriented nearly north-south developed along a baroclinic zone immediately inland from the shoreline of North Carolina. Prerequisite to the onset of coastal frontogenesis is the presence of low-level cold air pooled against the eastern slopes of the Appalachians (Bosart et al. 1972; Bosart 1975; Keeter et al.1995). In this case, the surface cyclonic circulation associated with Floyd, combined with lower pressure along the coast, forced cooler air to move down to near the coast east of the Appalachian Mountains over eastern North Carolina. These conditions were similar to the regional cold air-damming scenario associated with Tropical Storm Agnes (Bosart and Dean, 1991). On 15 September, frontogenesis commenced over extreme eastern North Carolina as confluence along the baroclinic zone sharpened. The increase in geostrophic flow over the ocean, as well as ageostrophic flow over land, contributed to baroclinic intensification as Floyd approached North Carolina over the course of the day. The front remained nearly stationary until approximately five hours before landfall.

MM data collected across the coastal front revealed a large thermodynamic differential five hours prior to landfall; T, T_d, and θ_e, spanning a distance of ~5 km were 2.1°C, 1.5°C, and 9 K, respectively. Mass convergence was significant along the

boundary, and strengthened to an order of magnitude 10^{-3} s^{-1}, as the hurricane drew closer to shore. The strong convergence enhanced lift along the boundary. As the eye of Floyd approached Cape Fear, NC, the front surged eastward. In situ data collected by the MMs indicate that colder and drier became laterally entrained into the western eyewall of Floyd.

Analysis of the 0600 GSO sounding revealed a 115-mb depth to the cold air west of the coastal front. East of the boundary, the MHX sounding contained a warm moist airmass with a convectively unstable layer. Cross-sectional analysis of potential temperature, in conjunction with VAD data, suggests that strong isentropic lift and warm air advection was occurring. As the hurricane traveled immediately east of the north-south oriented front, deep-layer easterly flow normal to the boundary developed, maximizing mesoscale ascent. WSR-88D data from LTX indicated a persistent contiguous frontal precipitation band. The juxtaposition of frontal orientation and deep layer flow resulted in rainfall >48 cm over portions of North Carolina. The greatest area of total rainfall occurred along and west of the boundary.

As Floyd traveled north toward Cape Fear, NC, the eye tracked immediately adjacent to and east of the frontal precipitation band, exerting an apparent entraining effect on the boundary. Four and a half hours before landfall, the frontal precipitation band was observed to move eastward and bow in toward Floyd's center on the west and southwest quadrants. A ragged asymmetric eye ensued and began to rapidly fill with precipitation two hours prior to landfall. The eye had completely filled a full hour before landfall. The apparent weakening of the system was quantified by a 4-mb increase in the

minimum central pressure as precipitation echoes filled the eye. Also at this time, in situ dropsonde data collected across the northeast to northwest quadrants of the system indicate that the hurricane circulation began laterally entraining the coastal front before the storm center came ashore. A frontal zone with a pronounced frontal inversion resided in the westernmost portion of the eyewall, containing a layer of relatively cold air 1 km-deep from the surface to 850 mb. Dropsonde data obtained in the east and northeast quadrant of the hurricane, in conjunction with surface data, indicated the cold air had been wrapped into the northeast quadrant 30 minutes after landfall. Approximately two and a half hours after landfall, the center of Floyd, in the lowest one kilometer, appeared to have become secluded and resided within a strong baroclinic zone.

This thesis has demonstrated that thermodynamic and kinematic interactions between the frontal boundary and the landfalling hurricane contributed significantly to large rainfall amounts over southern North Carolina. The front acted as a conduit, persistently lifting moist tropical air over the boundary, thereby producing heavy convective precipitation. The interactions appear to have augmented a rapid transport of relatively cold and dry continental air into the tropical system, resulting in a diminishment of hurricane intensity as the storm moved ashore.

From an operational standpoint, forecasters are encouraged to take into account the presence of a coastal front in concert with a tropical system when attempting to judge possible locations of maximum precipitation. Consideration of the effects such a boundary may have on the strength of a tropical system, as well as the depth of cold air

west of the surface discontinuity, may also aid in determining hurricane intensity at landfall.

Further investigation is required to substantiate the apparent effects of coastal fronts on landfalling hurricanes. Additional inquiry could also provide valuable information regarding the relative degree of interaction and effect between a landfalling hurricane and a pre-existing front, depending on geographical point of contact as well as angle and trajectory. Future efforts should include the study of previous and future U.S. landfalling hurricanes to verify common consequences resulting from any interaction with a coastal boundary.

5.2 Recommendations

To improve future operations of hurricanes several suggestions are put fourth. For field efforts designed to investigate baroclinicity within the eyewall of a landfalling hurricane, a minimum of four MMs are recommended when conducting the thermodynamic studies. Working in a storm relative framework, the MMs should be paired and positioned downstream of the eye with one pair in the northwest quadrant and the second pair, in the northeast quadrant. The sampling approach should have each pair working independently, transecting their respective quadrants normal to the eye's direction of movement. If a baroclinic zone is detected, both pairs of MMs should converge on the boundary, operating normal to the gradient. All cars remain mobile unless dictated by conditions.

At the time of landfall, all four MMs should perform transects normal to the eye's direction of motion and across the eye. If continuous transects are not possible, the cars should be positioned with one car each in the west, northwest, north and northeast of the eye. Once the eye has passed over the cars, transects should continue across the back side of the system and normal to the eye's direction of motion.

REFERENCES

Ballentine, R. J., 1980: A numerical investigation of New England coastal frontogenesis. *Mon. Wea. Rev.*, **108,** 1479-1497.

Bell, G. D., and L. F. Bosart, 1988: Appalachian cold-air damming. *Mon. Wea. Rev.,* **116,** 137-161.

Bluestein, H. B. 1993, *Synoptic-Dynamic Meteorology in Midlatitudes*. Vol. II, New York: Oxford University Press, 251-253 pp.

Bosart, L. F., 1975: New England coastal frontogenesis. *Quart. J. R. Met. Soc.,* **101,** 957-978.

_____, 5 December 2000, personal communication, State University of New York at Albany, Albany, NY.

_____, and D. B. Dean, 1991: The Agnes rainstorm of June 1972: Surface feature evolution culminating in inland storm redevelopment. *Wea. Forecasting*, **6,** 515-537.

_____, and E. H. Atallah, 2000: Extratropical transitions: Large-scale aspects. Preprints, *24th Conf of Hurricanes and Tropical Meteorology*, Ft. Lauderdale, FL, Amer. Meteor. Soc., 284-285.

_____, C. J. Vaudo, and J. H. Helsdon, Jr., 1972: Coastal frontogenesis. *J. Appl. Meteor.*, **11,** 1236-1258.

Bryan, G. H., and J. M. Fritsch, 2000: Moist absolute instability: the sixth stability state. *Bull. Amer. Meteor. Soc.,* **81,** 1207-1230.

Crum, T. D., and R. L. Alberty, 1993: The WSR-88D and the WSR-88D Operational Support Facility. *Bull. Amer. Meteor. Soc.,* **74,** 1669-1687.

_____, _____, and D. W. Burgess, 1993: Recording, archiving, and using WSR-88D data. *Bull. Amer. Meteor. Soc.,* **74**, 645-653.

Donall, E. G., M. A. Shapiro, and P. J. Neiman, 1991: Frontogenesis in a rapidly intensifying extratropical marine cyclone. Preprints, *First International Winter Storm Symp.*, New Orleans, LA, Amer. Meteor. Soc., 393-397.

Forbes, G. S., R. A. Anthes, and D. W. Thompson, 1987: Synoptic and mesoscale aspects of an Appalachian ice storm associated with cold-air damming. *Mon. Wea. Rev.,* **115,** 564-591.

Fujita, T. T., 1955: Results of detailed synoptic studies of squall lines. Tellus, **7,** 405-436

_____, and H. A. Brown, 1958: A study of mesosystems and their radar echoes. *Bull. Amer. Meteor. Soc.*, **39,** 538-554.

_____, and H. R. Byers, 1977: Spearhead echo and downburst in the crash of an airliner. *Mon. Wea. Rev.*, **105,** 129-146.

Garner, S. T., 1999: Blocking and frontogenesis by two-dimensional terrain in baroclinic flow. Part I: Numerical experiments. *J. Atmos. Sci.*, **56,** 1495-1508.

Keeter, K. K., S. Businger, L. G. Lee, and J. S. Waldstreicher, 1995: Winter weather forecasting throughout the Eastern United States. Part III: The effects of topography and the variability of winter weather in the Carolinas and Virginia. *Wea. Forecasting,* **10,** 42-60.

Keshishian, L. G., and L. F. Bosart, 1987: A case study of extended East Coast frontogenesis. *Mon. Wea. Rev.,* **115,** 100-117.

Kong, K.-Y., 2000: Detailed surface features associated with tropical storm Floyd (1999) at landfall. Preprints, *24th Conf of Hurricanes and Tropical Meteorology*, Ft. Lauderdale, FL, Amer. Meteor. Soc., 210-211.

Marks. F. D., and P. M. Austin, 1979: Effects of the New England coastal front on the distribution of precipitation. *Mon. Wea. Rev.,* **107,** 53-67.

Neiman, P. J., and M. A. Shapiro, 1993: The life cycle of an extratropical marine cyclone. Part I: Frontal-cyclone evolution and thermodynamic air-sea interaction. *Mon. Wea. Rev.*, **121,** 2153-2176.

_____, _____, and L. S. Fedor, 1991: Synoptic and mesoscale frontal characteristics within an intense extratropical marine cyclone. Preprints, *First International Winter Storm Symp.*, New Orleans, LA, Amer. Meteor. Soc., 108-114.

_____, _____, and _____, 1993: The life cycle of an extratropical marine cyclone, Part II: Mesoscale structure and diagnostics. *Mon. Wea. Rev.*, **121,** 2177-2199.

Rasmussen, E. N., J. M. Straka, R. Davis-Jones, C. A. Doswell III, F. H. Carr, M. D. Eilts, and D. R. MacGorman, 1994: Verification of the Origins of Rotation in Tornadoes Experiment: VORTEX. *Bull. Amer. Meteor. Soc.,* **75,** 995-1006.

Roebber, P. J., J. R. Gyakum, and D. N. Trat, 1994: Coastal frontogenesis and precipitation during ERICA IOP 2. *Wea. Forecasting,* **9**, 21-44.

Roux, F., 1988: The west African squall line observed on 23 June 1981 during COPT 81: Kinematics and thermodynamics of the convective region. *J. Atmos. Sci.*, **45,** 406-426.

Shapiro, M. A., and D. Keyser, 1990: Fronts, jet streams, and the tropopause. *Extratropical Cyclones, The Erik Palmén Memorial Volume*, C.W. Newton and E. Holopainen, Eds., Amer. Meteor. Soc., 167-191.

_____, E. G. Donall, P. J. Neiman, L. S. Fedor, and F. Gonzalez, 1991: Recent refinements in the conceptual models of extratropical cyclones. Preprints, *First International Winter Storm Symp.*, New Orleans, LA, Amer. Meteor. Soc., 6-14.

Simpson, R. H., 1974: The hurricane disaster potential scale. *Weatherwise*, **27,** 169 and 186.

Smith, T., 20 July 2000, personal communication, NSSL, Norman, OK.

Smull, B. F., and J. A. Augustine, 1993: Multiscale analysis of a mature mesoscale convective complex. *Mon. Wea. Rev.*, **121,** 103-132.

Straka, J. M., E. N. Rasmussen, and S. E. Frederickson, 1996: A mobile mesonet for fine-scale meteorological observations. *J. Atmos. Oceanic Technol.*, **13,** 921-936.

Taylor, G. I., 1938: The spectrum of turbulence. *Proc. R. Soc.*, **A164,** 476-490.

Trier, S. B., and E. B. Parsons, 1993: Evolution of environmental conditions preceding the development of a nocturnal mesoscale convective complex. *Mon. Wea. Rev.*, **121,** 1078-1098.

USDOC, 1999: *Storm Data.* Vol. 41, No. 9, Department of Commerce, 77-84 pp.

PERMISSION TO COPY

In presenting this thesis in partial fulfillment of the requirements for a master's degree at Texas Tech University or Texas Tech University Health Sciences Center, I agree that the Library and my major department shall make it freely available for research purposes. Permission to copy this thesis for scholarly purposes may be granted by the Director of the Library or my major professor. It is understood that any copying or publication of this thesis for financial gain shall not be allowed without my further written permission and that any user may be liable for copyright infringement.

Agree (Permission is granted.)

Disagree (Permission is not granted.)

_____ _____

Student Signature Date